

GIScience & Remote Sensing

ISSN: 1548-1603 (Print) 1943-7226 (Online) Journal homepage: www.tandfonline.com/journals/tgrs20

Revealing the influence of volcanic plumes on lake water quality parameters derived using remote sensing methods

Verity Flower , Dalin Jiang & Evangelos Spyrakos

To cite this article: Verity Flower , Dalin Jiang & Evangelos Spyrakos (2026) Revealing the influence of volcanic plumes on lake water quality parameters derived using remote sensing methods, GIScience & Remote Sensing, 63:1, 2754658, DOI: 10.1080/15481603.2026.2754658

To link to this article: https://doi.org/10.1080/15481603.2026.2754658

© 2026 The Author(s). Published by Informa UK Limited, trading as Taylor & Francis Group.

View supplementary material

Published online: 03 Nov 2026.

Submit your article to this journal

Article views: 73

View related articles

View Crossmark data

Full Terms & Conditions of access and use can be found at
https://www.tandfonline.com/action/journalInformation?journalCode=tgrs20

GISCIENCE & REMOTE SENSING
2026, VOL. 63, NO. 1, 2754658
https://doi.org/10.1080/15481603.2026.2754658

Taylor & Francis
by informa

RESEARCH ARTICLE

OPEN ACCESS Check for updates

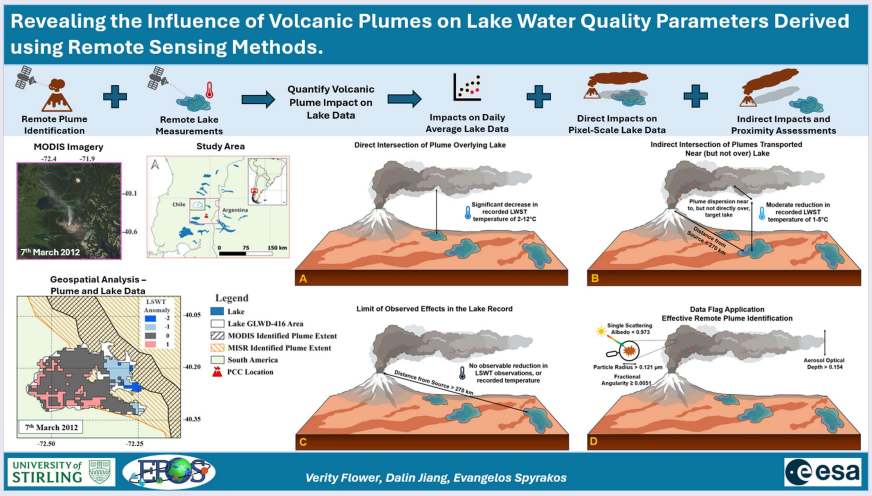
Revealing the influence of volcanic plumes on lake water quality parameters derived using remote sensing methods

Verity Flower, Dalin Jiang and Evangelos Spyrakos

School of Life and Environmental Sciences, University of Stirling, Stirling, Scotland, United Kingdom

ABSTRACT

Satellite-derived observations of inland waters are widely used in environmental monitoring, often forming the basis of long-term analyses in the absence of continuous in situ measurements. However, the influence of transient atmospheric phenomena, such as volcanic plumes, on these datasets remains insufficiently quantified. We investigate the impact of volcanic plumes generated during the 2011–2012 eruption of Puyehue-Cordón Caulle, on the availability of remotely observed lake data (lake surface water temperature [LSWT], turbidity and chlorophyll-a) compiled from the ESA Climate Change Initiative (CCI) Lakes dataset. We subsequently extend the assessment of LSWT observations, combining these with coincident plume observations from the Multi-angle Imaging SpectroRadiometer (MISR) and the Moderate Resolution Imaging Spectroradiometer (MODIS), to identify the impacts of diffuse volcanic plumes on remote lake observations. Linear mixed-effects models assessed plume effects, while accounting for lake-specific variability during plume events. These findings indicate that while existing cloud masking removes LSWT observations in the presence of dense ash-rich plumes, diffuse volcanic plumes frequently remain undetected while significantly impacting LSWT records. Plume impacts varied seasonally, with LSWT observations being lower in winter months, and warmer in summer. At the pixel scale, plume interference was associated with LSWT8 reductions of up to 12 °C beneath dense ash-plumes, and 1 °C–5 °C beneath diffuse plumes. Geographic conditions influenced overall data availability, with measurable effects extending to ~270 km from the volcanic source. A random forest classification achieved an overall accuracy of 78% classification accuracy for distinguishing plumes from cloud and background regions, demonstrating the potential to develop an automated flag for CCI Lake data. These findings demonstrate that diffuse volcanic plumes can introduce substantial uncertainty into satellite-derived LSWT observations, although the magnitude and spatial extent of the observed effects are case-specific. This highlights the need for further investigation across diverse volcanic events and geographical settings to support the development of dedicated quality flags for diffuse and transient aerosol features.



ARTICLE HISTORY

Received 9 June 2026
Accepted 21 October 2026

KEYWORDS

Random forest model; linear mixed effect model; transient atmospheric interference; volcanic plumes; remote water quality observations

CONTACT Verity Flower verity.flower@stir.ac.uk

Supplemental data for this article can be accessed online at https://doi.org/10.1080/15481603.2026.2754658.

© 2026 The Author(s). Published by Informa UK Limited, trading as Taylor & Francis Group.
This is an Open Access article distributed under the terms of the Creative Commons Attribution License (http://creativecommons.org/licenses/by/4.0/), which permits unrestricted use, distribution, and reproduction in any medium, provided the original work is properly cited. The terms on which this article has been published allow the posting of the Accepted Manuscript in a repository by the author(s) or with their consent.

1. Introduction

Lakes play a vital role in global water resource management, contributing to drinking water supply, agriculture, and ecosystem services. Monitoring these systems through in situ observations alone is often impractical due to cost, accessibility, and logistical constraints (Rickards et al. 2023). Satellite remote sensing therefore provides a critical alternative, enabling systematic monitoring of lake temperature, water quality, and extent at regional to global scales (Sajib et al. 2025; Sheffield et al. 2018; Zeng et al. 2025). However, volcanic plumes represent a particularly complex and variable form of atmospheric interference in these measurements. These plumes typically consist of mixtures of ash, sulfates, and water vapor, with properties that evolve both temporally and spatially throughout an eruption (Carey and Bursik 2015; Tournigand et al. 2019). Dense ash-rich plumes are generally identifiable in remote sensing imagery and removed through standard quality control procedures and cloud masks (Petracca et al. 2022; Robbins et al. 2022). Large volcanic plumes have also been successfully detected in high temporal-, low spatial-resolution data (Pavolonis, Sieglaff, and Cintineo 2018) and where plume have a notable ash component (Picchiani and Chini 2015). However, more diffuse plumes, particularly those dominated by fine particles or sulfate aerosols, may not be detected, despite having the potential to attenuate or distort surface signals (Katsev et al. 2021). This issue can be particularly relevant for satellite-derived observations of inland waters (Niroumand-Jadidi, Bovolo, and Bruzzone 2020).

Earth observations recorded by optical remote sensing instrumentation represent a significant resource for monitoring environmental phenomena and providing essential climate variables (ECVs), including lake water quality parameters (Ballari et al. 2023; Carrea et al. 2023). These data are increasingly used in isolation, deriving environmental characteristics from remote observations alone (Fensholt et al. 2015; Jiang et al. 2024; Kimball 2008). However, these data are also frequently employed to augment ground-based observation records, to provide a more extensive data series or infill data gaps to facilitate more accurate environmental assessment. A key source of uncertainty arises from transient atmospheric interference. Volcanic eruptions, wildfire smoke, dust storm and anthropogenic pollution introduce aerosols into the atmosphere that can alter the radiative signal received by satellite sensors (Kahn et al. 2023; Li et al. 2022). While operational processing chains typically include cloud masking algorithms (Carrea et al. 2023) to remove optically thick features, these approaches are not designed to consistently detect diffuse aerosol plumes. As a result, diffuse atmospheric particles that are not explicitly identified as clouds may still influence retrieved surface properties. With the increasing availability and use of online datasets of remote observations, understanding the impact of these transient events is imperative to prevent the inaccurate interpretation of evolving environmental conditions, such as lake water quality.

1.1. Study area

Within this study we will explore the challenges posed by the presence of volcanic plumes when monitoring lake water quality, particularly those plumes too diffuse to be screened out as cloud features by traditional remote sensing algorithms. We present evidence of how volcanic particles, held in atmospheric suspension, can impact lake water measurements provided in the CCI Lake database. To facilitate this, a persistent volcanic eruption, occurring over a lengthy but finite time period (~1 year), and in close direct proximity to numerous lakes, was required to effectively evaluate the impacts over a range of environmental conditions. The eruption of Puyehue-Cordón Caulle (PCC) (Figure 1) generated frequent plumes that dispersed widely across central Chile and Argentina was deemed to be an appropriate exploratory case study. PCC volcano, erupted on 4th June 2011, following a period of seismic activity in April–May 2011 (Bignami et al. 2014). The eruption produced persistent plumes, some reaching over 10 km in altitude, through until March 2012 (Maes et al. 2016). These plumes varied in altitude and extent across the eruption period but generally decreased in size as the eruption progressed (Bonadonna et al. 2015). Central Chile and Argentina contain many lakes with a wide range of physical characteristics (e.g. shape, size, depth, geographic location). PCC is located with the wider Puyehue-Cordón Caulle volcanic complex (PCCVC) in central Chile, a thin volcanic complex runs along the eastern border with Argentina with PCC located in the center (Lara et al. 2006). The PCCVC is characterized by a chain of volcanic peaks that dip to the plains of Argentina to the east and the Pacific Ocean to the west (Elissondo et al. 2016). Varying

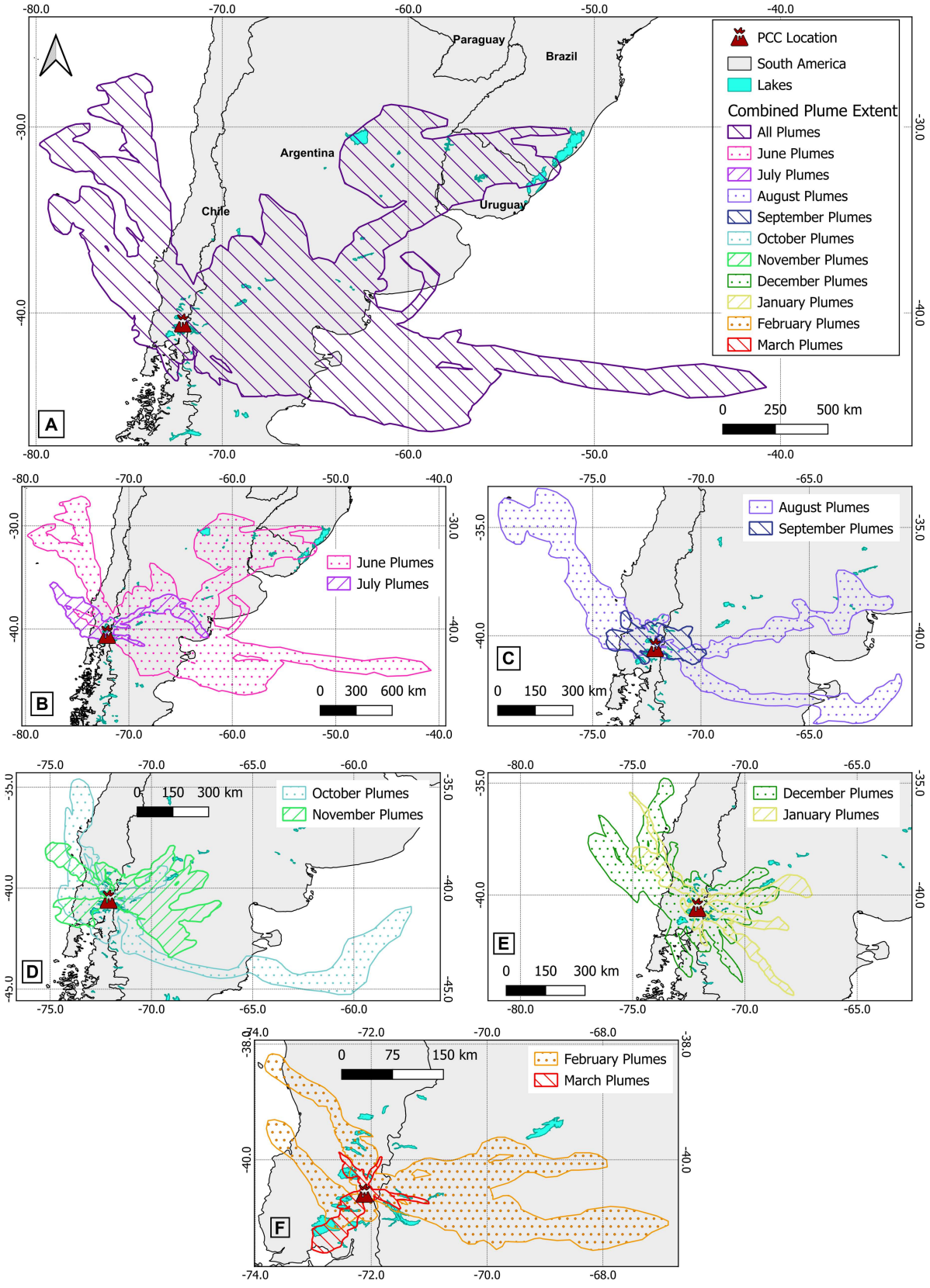


Figure 1. Location of MODIS-observed plumes emitted by PCC volcano (red volcano marker). Plumes are displayed as total combined observed extent (A); and also in pairs of months (B–F) during the eruption period (June 2011–March 2012). Lake locations (blue) are also noted across the analysis region with effected locations extending to: Chile, Argentina, Uruguay and Brazil.

atmospheric dynamics cause diverse patterns of dispersion with onshore winds from the Pacific dominating higher altitude plumes dispersed over Argentina (Figure 1A–D). While plumes emitted to lower altitudes, and when onshore winds were less dominant, are frequently transported to the north and west (Figure 1C–F).

Numerous lakes (17) are located within 1000 km of PCC volcano (Figure 1A) and were impacted by multiple plumes during the defined eruption period. These 17 lakes were incorporated into these analyses, based on relative impact, data availability and analysis function. All 17 were used to identify how the presence of volcanic plumes impacted the overall availability of observations of surface features. Eleven lakes, in close proximity to the volcano, were used to conduct statistical assessment of how the presence of plumes impacted daily lake observations. With a single lake selected for in-depth pixel-scale assessment due to the presence of multiple observation records corresponding to observed plume events. As this study represents an exploratory assessment of an opportunistic volcanic eruption event, the lakes were not intended to constitute a statistically representative sample of lakes globally. Consequently, the findings should be interpreted in the context of lakes exposed to volcanic plumes during the PCC eruption, rather than as directly generalizable to all lakes or volcanic events.

1.2. Research gap

Despite considerable advances in atmospheric correction and cloud masking algorithms, the influence of diffuse volcanic plumes on remote measurements of inland water quality remains unquantified. Existing cloud-screening procedures are broadly effective at removing optically thick plumes (Pavolonis, Sieglaff, and Cintineo 2018; Picchiani and Chini 2015) but are not optimized to identify diffuse aerosol plumes that allow surface reflectance to transit through to a sensor, but which may have a significant impact on the signal intensity reaching the satellite-based sensor. Consequently, it remains unclear whether volcanic plumes can lead to systematic bias in the lake record derived from space-based observations, how significant these biases may be and whether there are spatial or seasonal variations in the impacts observed. Within this work, we use the persistent eruption of PCC to identify the effect of diffuse atmospheric particles on satellite-derived lake water quality indicators, primarily LSWT. Addressing these knowledge gaps is essential as satellite-derived lake water quality records are increasingly used for long-term lake studies, and no studies currently exist that explore the direct impacts of diffuse volcanic plumes on these measurements.

1.3. Aims

Within this study there are three primary aims that will be addressed through a range of visual and statistical assessments:

1. To establish the impact of volcanic plumes on the remote observations of lake quality variables, and the extent of this influence.
2. To identify if volcanic plumes can be distinguished from background observations and/or cloud features based on MISR particle property observations to facilitate the automated flagging of impacted lake data.
3. To quantify the impact that volcanic plumes can have on remote lake quality observations.

2. Methods

Plume observation frequency is a critical factor in the ability to establish the impact of volcanic plumes that is outlined in this work. While instruments with unique observing characteristics (e.g. multi-angle observations) may provide novel insights in environmental assessment, their overall coverage can be limited by a more restricted overall swath width increasing time between observations. This can lead to gaps in the observational record (Figure 2Aii) which, when paired with the sporadic nature of volcanic eruptions, can be less than ideal for assessing overall eruption impact. Therefore, in this work we combine unique multi-angle observations from the MISR instrument, with wider context imagery incorporated from the Moderate Imaging Spectroradiometer (MODIS) instrument (Figure 2Ai). Both instruments are housed on the Terra platform (Salomonson et al. 1989), which was launched into a sun-synchronous orbit in December 1999

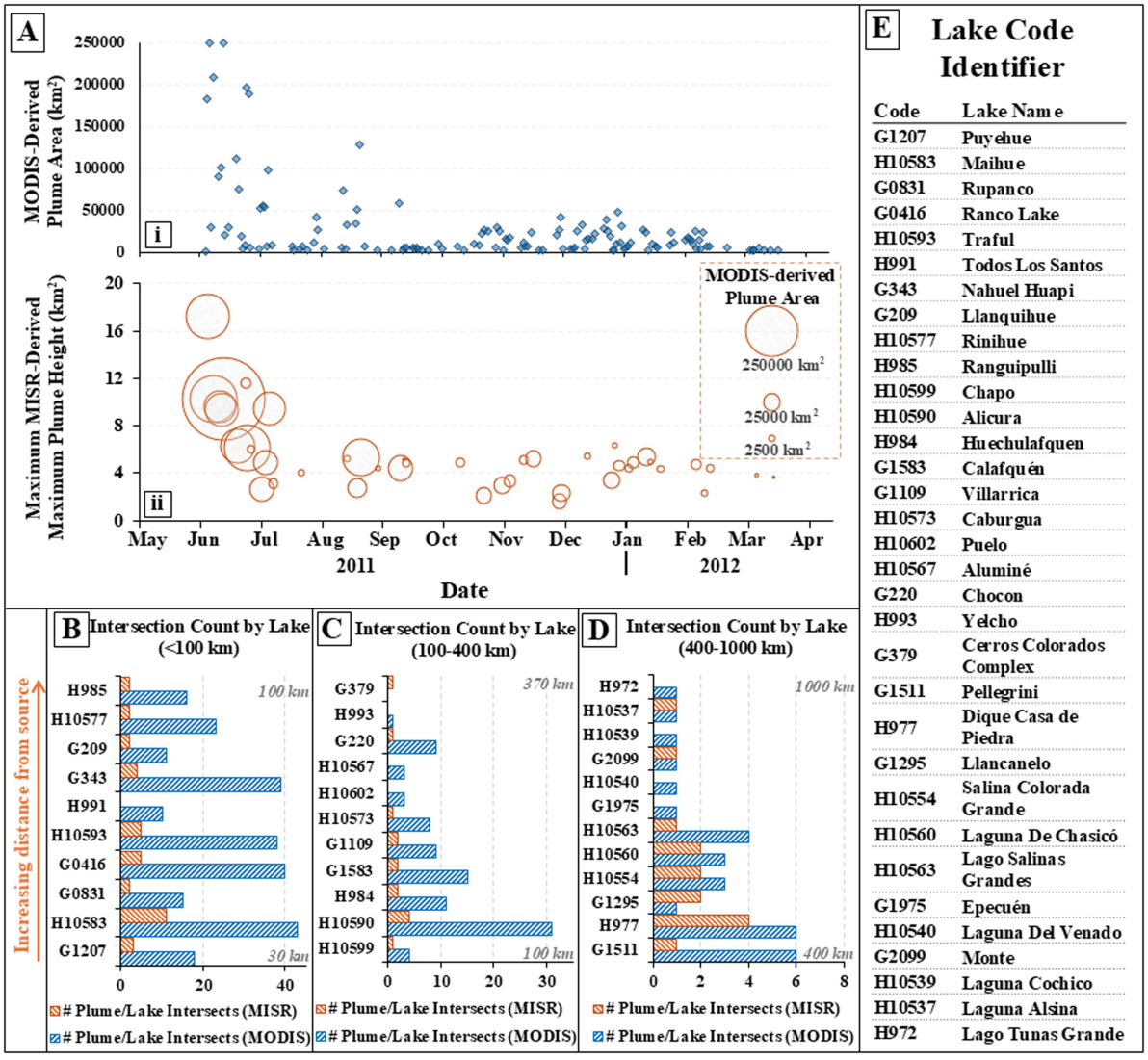


Figure 2. (A) (i) Timeline of MODIS-derived plume area during the PCC eruption period (June 2011–April 2012); (ii) marker representing MISR-derived maximum plume heights (y-axis) and MODIS-derived plume extent (marker size) for concurrently observed plume; (B–D) graphical representations of the instances in which volcanic plumes were observed to obscure lakes (fully or partially) in the PCC-impacted region, intersection values are segregated to denote MODIS (blue hash marking) and MISR (orange hash marking) observations, and are listed in increasing distance from the source (start and end distances noted in gray on each plot); (E) list of lake names associated with codes used in (B–D).

with a day-time equator crossing of ~10:30 local time. Consequently, these instruments collect coincident observations in the nadir direction, with a history data set spanning over a 24-year period.

2.1. Remote plume data

2.1.1. MISR

MISR is a passive, visible-near infrared (VIS-NIR) sensor, measuring upwelling shortwave radiance across four spectral bands (446, 558, 672, and 866 nm; Diner et al. 1998). MISR operates nine cameras collecting near-coincident imagery across multiple viewing angles. Observations are obtained as fixed angles of nadir, plus four additional view angles in the forward (F) and aft (A) directions (26.1°, 45.6°, 60°, 70.5°), relative to the orbit track (Diner et al. 1998). The observations are recorded across a common swath of ~380 km at a spatial resolution of 1.1 km in each spectral band. Limited improved resolution (275 m) is available for all spectral bands in the nadir camera, and additionally for the red spectral bands in each of the other eight cameras

(Diner et al. 1998). MISR data can facilitate the calculation of geometrically derived plume heights, accompanied by associated wind vectors, calculated from the multiangle imagery where there is sufficient contrast among the plume pixels (Moroney, Davies, and Muller 2002; Muller et al. 2002; Kahn et al. 2007; Nelson et al. 2008, 2013; Scollo et al. 2012). These plume heights have been found to be more stable over time than their radiometrically derived equivalents from other sensors (Flower and Kahn 2017a). While MISR is not sensitive to the extremely diffuse particles that can be retrieved with active LiDAR measurements, MISR's wider swath width provides a better synoptic view that provided by LiDAR (Flower and Kahn 2017a). The MISR Interactive eXplorer (MINX) software package (Nelson et al. 2008, 2013) facilitates the manual classification of plume areas observed in MISR imagery, whilst also calculating the plume heights and wind vectors derived through analysis of the plume motion occurring between the extreme forward and aft camera observations (~7 min). Since volcanic eruption classification commonly associate plume altitude with explosivity (Newhall and Self 1982), these observations can be used to assess eruptive dynamics. Additionally, the plume areas defined during the MINX analysis will be saved for inclusion into investigation of plume/lake intersections, that will be conducted in the geospatial data platform QGIS (QGIS.org 2025).

Particle microphysical properties can be derived radiometrically from the multiangle, multispectral MISR data (Kahn and Gaitley 2015; Kahn et al. 2010; Limbacher and Kahn 2017; Martonchik, Kahn, and Diner 2009) using the MISR research Algorithm (RA) (Limbacher and Kahn 2014, 2017). These observations can facilitate the distinction of particle evolution within individual plumes, as well as ongoing variations between plumes as an eruption progresses (Flower and Kahn 2021). These data provide four derived variables that are used within this work to track relative variations in properties within and between plumes, clouds and background: Aerosol Optical Depth (AOD); Retrieved Effective Particle Size (REPS); Retrieved Effective Particle Absorption (REPA), which is analogous with Single Scattering Albedo (SSA) in this work; and Fraction of Non-Spherical Particles (FNSP). For the purposes of this work, we will be reporting the general variations in these observations between eruptive plumes. While it is beyond the scope of this work to provide detailed plume analyses, further work on plume particle classification is ongoing. For selected examples of MISR RA output for PCC, see the associated supplementary material provided with this paper. For full details of the MISR RA outputs, please see the associated data repository at – Cordon Caulle Plume Data (2011–2012) – MISR/MODIS Satellite Retrievals.

2.1.2. MODIS

MODIS is a broad-swath, visible-infrared (VIS-IR) imager providing global coverage every 1–2 days (Salomonson et al. 1989; Wright et al. 2002). MODIS was designed for a range of applications, here we will be exploiting its capabilities in the visual spectrum to highlight the existence and dispersion of volcanic plumes at a synoptic scale. Facilitated by a swath width of 2330 km MODIS can provide additional context of the horizontal extent of plumes complementing MISR data (Vermote et al. 2007; Xiao et al. 2009). Since the MODIS and MISR sensors are both housed on NASA's Terra satellite platform, the observations are concurrent (at the nadir view) and so MODIS can provide directly comparable synoptic scale information for the smaller spatial extent observations obtained by MISR. Additional MODIS observations will be used in the assessment of CCI Lake data to assess the presence/absence of plumes above individual lakes, where MISR data is unavailable. A review was completed of all available MODIS data, at each individual lake analyzed, to visually identify if there was a plume present over, or near, the lake. Plume identification was undertaken through direct visual inspection of each MODIS image by an experienced volcanological remote sensing scientist, rather than through an automated classification procedure. Each image was reviewed individually to identify the spatial extent of the visible plume and to distinguish the plume from surrounding background areas and cloud. The plume region was delineated where it could be visually distinguished from the surrounding scene, while areas: obscured by cloud; instances where other interferences were observed (e.g. wildfire plumes); data errors existed; or where plume boundaries could not be reliably identified, were noted for subsequent analyses to prevent convoluting these factors with the impacts of volcanic plumes. No automated plume-detection or classification procedure was used. A second MODIS sensor, launched on the Aqua satellite in 2002, provides additional daily observations, ~3 h later at the equator than the Terra overpass and was incorporated into this analysis during the manual plume identification process as gap filling, where there were issues with the Terra-based observations (e.g. missing data tiles, cloud obscured observations when lake data suggests visibility was clear).

2.2. ESA climate change initiative (CCI) lakes data

We leverage the ESA Climate Change Initiative (CCI) Lakes project's long-term, multi-variable dataset of lake properties as a basis for our analysis (Carrea et al. 2023). The lake data, derived from satellite observations, includes lake surface water temperature (LSWT), turbidity, chlorophyll-a (Chl-a) concentration, lake extent, and water level (https://climate.esa.int/en/projects/lakes/, Carrea et al. 2024). In this study, the ESA CCI Lake database version 2.02 was used. The ESA CCI Lakes dataset is a multi-sensor climate data record designed to provide consistent and homogeneous observations over time, incorporating processing and inter-sensor consistency measures where applicable (Carrea et al. 2023). Nevertheless, residual inconsistencies associated with changes in sensor characteristics or processing cannot be entirely excluded. The ESA CCI Lakes Level-3 LSWT product has a reported per-pixel uncertainty of approximately 0.4 °C–0.7 °C under clear-sky conditions, with larger uncertainties potentially arising near lake-land boundaries (Simis et al. 2025). Consequently, plume-induced anomalies substantially exceeding this uncertainty are unlikely to arise solely from retrieval error. The ESA CCI Lakes LSWT product applies operational atmospheric correction and cloud screening algorithms to convert top-of-atmosphere thermal radiance into lake surface water temperature (Carrea et al. 2023). Only observations passing the ESA CCI Lakes quality-control criteria were retained for analysis. Pixels identified as cloud-contaminated by the operational cloud mask were automatically excluded prior to the data download process. Because the operational processing chain is optimized for typical atmospheric absorption and cloud contamination rather than volcanic aerosols, it is expected that residual plume contamination remains within observations, that otherwise satisfy standard quality-control criteria. Therefore, the obtained CCI Lake observations were subsequently classified as plume-impacted or non-impacted by visual inspection of coincident MODIS true-color imagery and MISR aerosol products. CCI Lake observations are associated with a “pinned observation time” of 12:00 UTC. However, since they are compiled from multiple polar-orbiting satellites (ATSR-2, AATSR, MODIS [Terra], AVHRR [MetOp-A, MetOp-B], SLSTR-A, SLSTR-B) their specific observation time can vary but is generally expected to fall between 10:00 and 13:00 local time (Carrea et al. 2023) comparable to the observation times of MODIS/MISR imagery. Consequently, any statistically significant differences identified between plume and non-plume observations are interpreted as limitations of the current operational processing rather than necessarily indicating deficiencies in the underlying lake temperature retrieval algorithm.

While the data are generated at a nominal pixel scale of ~1 km, we also generated mean daily values for each target lake, with associated standard deviations. The pixel-scale data were used to investigate the direct impact of plumes using geospatial techniques (QGIS.org 2025) while daily averages were used in the generation of time series to assess overall plume impacts. The data record spans 21 years of daily observations (2000–2020, inclusive). Daily averages were collated for LSWT, Chl-a and turbidity for each identified lake. A standard monthly baseline for individual lakes of each observation type (LWST, Chl-a and turbidity) was calculated by excluding the PCC eruption period (Jun 2011–Apr 2012) and calculating corresponding means and standard deviations of the remaining observations. These lake-specific baselines were used to calculate standardized data anomalies, facilitating the intercomparison of the relative plume impact between lake systems. Pixel-scale data were employed to generate a comprehensive understanding of the direct impacts of plumes on corresponding lake data. In total, 33 lakes were observed to be impacted by at least one plume (Figure 2B–E), of which 17 were impacted by multiple plumes and were included for more detailed analysis.

2.3. Statistical analyses

Statistical assessments were undertaken to evaluate the significance of the patterns identified through visual interpretation. These analyses focused on LSWT, as the existing flagging procedures were generally effective for Turbidity and Chl-a, leaving insufficient observations for comparable statistical assessment of these variables. LSWT therefore provided the primary dataset for investigating the potential influence of volcanic plumes on satellite-derived lake observations.

All statistical analyses were conducted using codes created in R and run in RStudio (R Core Team 2025). These were employed in the determination of the potential for a data flag to be included in the CCI data (random forest classification: RF) to alert end users as to whether the data being used is impacted by

transient plumes. While a second method (linear mixed-effects modeling: LMM) was employed to assess the statistical relevance of the lake values identified outside of historical expected ranges during visual assessment. The methods employed are detailed below and the relevant R codes can be found in the supplementary material provided with this manuscript.

2.3.1. Flagging procedure—random forest analysis

Statistical assessment of environmental data, which is typically characterized by non-linear, complex dynamics, with frequent missing values, can be challenging for traditional linear methods (Cutler et al. 2007; De'ath and Fabricius 2000). However, RF models have been found to be effective in the classification of environmental characteristics and dynamics (Breiman 2001; Cutler, Cutler, and Stevens 2012). These have also been found to be capable in the quantitative analysis of volcanic plumes in both the laboratory experiments (Rayborn and Jellinek 2022) and remote observation studies (Corradino et al. 2024; Romeo et al. 2023). An RF model was employed here to identify if the available MISR RA data could be employed to create an automated flag for the CCI Lake database. The aim of this flag would be to indicate observations that are likely to be impacted by presence of transient atmospheric plumes that were not removed by existing cloud masking procedures. Data for the observed plumes, associated background and cloud values were compiled for each MISR observation date. Background data was taken from all MISR observations, while cloud features were analyzed opportunistically when identified as being present in the region around the plume area during the visual review (full data records available in the Data repository for this work: Cordon Caulle Plume Data (2011–2012) – MISR/MODIS Satellite Retrievals). The RF model was selected due to its capabilities to generate a multi-parametric decision tree incorporating multiple particle characteristic (e.g. plume depth, size, shape, scattering/absorption). RF models offer good predictive capabilities without the need for extensive tuning (Fox et al. 2017).

Following initial data cleaning (removal of null; saturation point and missing values) for the 4 key variables derived with MISR (AOD, REPA, REPS and FNSP) was completed. Initially a total of 50,000 observations (of 700,000 possible) were randomly selected for model development using a fixed random seed to ensure reproducibility. However, this was subsequently extended to sample sizes of 100,000 and 350,000, to ensure the optimum data threshold had been met for the generation of an effective model (Silvey and Liu 2024). The significant increase in included samples was expected to improve accuracy, and increase the number of cloud observations that were included in the sample set, considering these only represent ~8% of the total observations The final dataset comprised three classes (Plume, Background and Cloud), with the number of observations in each class incorporated into the sampled dataset (Sample Count 50 K:100 K:350 K—Background—20357:40547:141822; Cloud—3881:7783:27587; Plume—25762:51670:180591). Model performance was evaluated using stratified 10-fold cross-validation, ensuring that the class proportions were maintained within each fold. In each iteration, approximately 90% of the data were used for model training with the remaining 10% employed validation, with every observation serving as validation exactly once across the ten folds.

An RF classifier incorporating 500 decisions trees was employed, each trained on a different random subset of the data. While each decision tree predicted the classes (Plume, Background and Cloud) the final output reported is the result of averaged class probabilities across the individual analyses. Classification performance was assessed from the aggregated cross-validated predictions, using results derived from the resulting: confusion matrix; overall accuracy; Cohen's kappa; and one-versus-rest receiver operating characteristic (ROC) curves; with corresponding area under the curve (AUC) values. A final RF model was subsequently fitted to the complete sampled dataset to derive variable importance estimates.

2.3.2. Linear mixed-effects modeling (LMM)

To effectively test whether the presence of transient volcanic plumes had a statistically significant impact on the remote lake measurement, we employ an LMM. The LMM model was selected as it can deal with repeated, but non-regular, observations (Bolker et al. 2009 Schielzeth et al. 2020), ultimately allowing both population-level effects (e.g. the overall influence of plume presence) and lake-specific variations to be estimated simultaneously. LMMs have been used in the analysis of a variety of environmental processes, including relating to lakes (Lessels and Bishop, 2013; Vera Mercado and Engel 2021), and volcanic emissions (Auchmann et al. 2013; Laiolo et al. 2016). Here, the ability of LMMs to deal with both fixed and random effects make them more appropriate that the more limited single linear regression model, which would not

be able to account for the inter-lake variability identified in this analysis (Zuur et al. 2009). Facilitating the inclusion of independent baselines for each lake analyzed.

Prior to implementation of the LMMs, corresponding MISR/MODIS data was used to identify if LSWT observation dates (at each of 11 lakes) were impacted (plume present) or non-impacted (no plume present) by visible volcanic plumes. A second binary classification was also included to identify if Clouds were present or not over the corresponding lake, based on visual identification of cloud features during the plume presence review. LSWT observations from each lake were initially compared with lake-specific monthly climatological means to calculate temperature anomalies. Anomalies were then standardized by dividing by the corresponding monthly standard deviation, producing a standardized anomaly (z-score) for each observation. Because lakes differ substantially in their typical seasonal temperature regimes, analyses were performed on these standardized temperature anomalies, rather than raw lake surface temperatures. Standardization relative to each lake's monthly climatology allowed the effects of atmospheric plume exposure to be compared across lakes on a common scale, independent of differences in absolute temperature or seasonal variability. Standardized anomalies greater than ±2 standard deviations were classified as extreme events. These standardized anomalies were then assessed with the LMM to quantify if the impacts of plumes, and clouds, on lake quality measurements were statistically significant.

This analysis was subsequently extended to establish whether the influence of atmospheric plumes varied seasonally through the inclusion of a model including the interaction between plume presence and month. Type III analysis of variance (Anova) with Satterthwaite's approximation for denominator degrees of freedom, were used to assess the significance of main effects and interactions. Estimated marginal means were calculated for plume and non-plume observations overall and separately for each month. Pairwise comparisons between impacted and non-impacted observations within each month were used to identify periods during which atmospheric plumes were associated with the largest changes in LSWT anomalies. Ninety-five percent confidence intervals were calculated for all estimated effects. Model assumptions were evaluated by inspecting residual diagnostics, including residual normality, homoscedasticity, influential observations and model singularity. Model coefficients, confidence intervals and estimated marginal means were used to quantify the magnitude and direction of plume effects. In addition to the LMM analysis, contingency tables comparing the proportion of observations exceeding ±2 standard deviations between impacted and non-impacted conditions were analyzed using chi-square and Fisher's exact tests. The output of these analyses have been compiled and included in supplementary material provided with this manuscript.

3. Results

The following section will summarize the remote-sensing observations that were derived in this work and subsequently incorporated into statistical and geospatial analyses, discussed in Section 4.

3.1. Plume observations

Remote investigation of the 2011–12 eruption of PCC resulted in the identification of 39 plumes with the MISR sensor (Figure 2Aii). Gaps in the plume observations were noted during this initial analysis (Jul–Aug & Sep–Oct 2011). MODIS was used to establish if these plume data gaps resulted from: quiescence in the volcanic eruption; observation errors associated with the non-global daily coverage of MISR; or an artifact of extensive cloud cover over the region. The daily assessment of MODIS observations (Figure 2Ai) highlighted that while cloud cover did impact plume observation periodically, consistent data gaps were not identified to align with the MISR record. MODIS data facilitated the assessment total nadir-visible area of the plumes, concurrent with the MISR observations (Figure 2Aii).

Ultimately multiple phases within the eruption were identified for this review (Phase 1: Jun–7 Jul; Phase 2: 14 Aug–12 Sep; Phase 3: 13 Sep–14 Feb) interspersed with inter-phase periods characterized by small near-vent plumes (Figure 2Ai):

Phase 1: MISR plume heights (Figure 2Aii) indicate that Phase 1 was characterized plumes that reached an altitude of up to 17 km (Figure 2Aii). These large (average—1,15,000 km^2: Range—1600–6,65,000 km^2), high altitude (Average—8.7 km; Range—2.7–17.2 km), events rapidly diminished, with plumes being confined below

an altitude of 6 km after the 6th July (31 days after first MISR-imaged plume) (Figure 1B). After the 6th July observations also become more sporadic with MISR (Figure 2A) suggesting a shift in eruption dynamics around this time. In a volcanological context, these periods of quiescence could relate to a reduction in the rate of magma upwelling in the subsurface conduits, increasing the time between explosive events and corresponding observed plumes (National Academies of Sciences (NAS) et al. 2017).

Phase 2: the second phase encompasses plumes emitted between 14th August and 12th September (Figure 2A). These show small to moderate plume extent (average—28,000 km^2: range—350–1,29,000 km^2) (Figure 1C). While these plumes occur within a distinct time period and display similar ejection altitudes the plumes themselves show two distinct size groupings. Three of these plumes are more comparable in size to the earlier eruption period (average—72,603 km^2: range—32,000–1,29,000 km^2), with the remaining plumes displaying an order of magnitude decrease in size (average—1900 km^2: range—370–3600 km^2), more characteristic of plumes emitted after September 2011.

Phase 3: the final phase (after 13th September 2011) is characterized by small eruption plumes (average—10,400 km^2: range—511–2600 km^2) (Figure 1D–F) emitted at or below 5 km in altitude (Figure 2Aii). While the plume altitude does not show the typical exponential decrease that would be the result of the expected reduction in explosive energy associated with the end of an eruption (Sparks et al. 1997; National Academies of Sciences, Engineering, and Medicine, 2017), the plume size does highlight a shift to smaller plumes over time, particularly evident after 19thJanuary 2012 (Figure 1E–F).

Overall, the emissions from PCC appear to shift from more explosive ash-rich eruptions (e.g. those containing larger, angular more absorbing aerosol components) to more effusive water/sulphate dominated plumes (e.g. those comprised of small, spherical, non-absorbing aerosols) based on review of existing literature (e.g. Bignami et al. 2014), and visual assessment of plume observations derived from the Multi-angle Imaging SpectroRadiometer (MISR) used in this work (selected examples available in the Supplementary material: For full plume results see data repository: Cordon Caulle Plume Data (2011-2012) – MISR/MODIS Satellite Retrievals). Local ground-based monitoring stations measuring PM10 levels, frequently exceeding daily and annual limits up until January 2012 (Elissondo et al. 2016), however plumes continued to be observed until March 2012 (Figure 2a), suggesting the final months of the eruption (January–March 2012) were dominated by sulfate/water plumes instead of the ash-rich emissions observed before January 2012.

3.2. Plume–lake intersections

The MODIS plume review identified ~390 plume–lake intersections, across 33 lake systems, for possible analysis in this work. Some of the lakes identified were impacted by a single long-range plume while other lakes near to PCC were impacted across the entire eruption period. Plumes extended across: Chile, Argentina, Uruguay and Brazil (Figure. 1). However, the reduction in plume dispersion extent during the eruption, meant that lakes in Brazil and Uruguay were only impacted in June, the first month of the eruption (Figure 1B). Ultimately, 17 lakes were identified in Chile and Argentina to have been impacted by more than one MISR-observed plume (Figure 2B–D). Eight of the lakes, spanning a range of distances from the volcano (35–185 km), were used to visually evaluate the impact of plumes on the daily CCI Lake observations (Figure 3). However, 11 lakes were identified to be impacted by multiple plumes and located within 1000 km of the volcano, making them appropriate for the statistical assessment of plume impacts on lake observations (Section 4.2). Finally, Lake Ranco (GLWD_416) was selected for detailed investigation of the pixel-scale impacts on CCI lake observations. Lake Ranco was selected as it had the highest frequency of MISR-plume observations, that correlated to available lake observations (Figure 2B), from which to assess the direct impact on lake observations (6). While one lake, Maihue (HYLA_10583), had more plume intersections (12; Figure 3), this location had more lake data masked out by the existing cloud mask, reducing the efficacy of using this location for detailed pixel-level analysis.

3.3. CCI lake data review

Lake CCI data (LSWT, Chl-a, Turbidity) was collated for the 17 lakes with a range of plume–lake intersections identified. Overall, LWST was the most likely variable to be provided by the database, with Turbidity and Chl-a retrieval rates around 50% less than LWST. This initial analysis highlighted that the CCI cloud screening procedure,

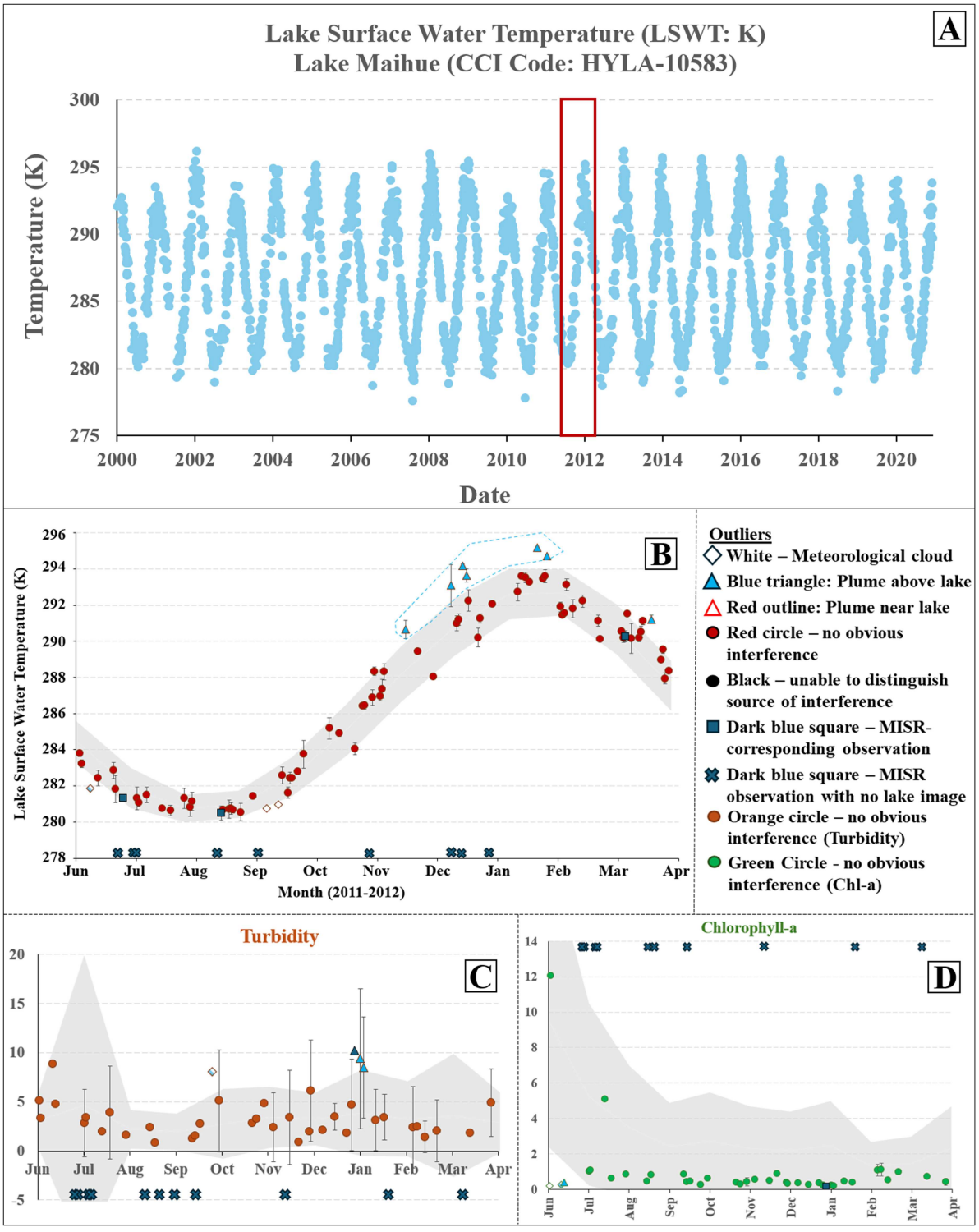


Figure 3. In depth analysis of Lake HYLA-10583: (A) 20-year LSWT records; and 2011–2012 observations overlaid on derived "typical" values (generated the average and standard deviations at individual lakes during non-eruptive years: grey) for (B) LSWT; (C) Turbidity; and (D) Chlorophyll-a.

that removes data when clouds are present and flags data errors, appears to be effective with 75% of MISR-observed plume days being removed from the LWST data record and 90% screen out in the Turbidity and Chl-a data (e.g. Figure 3C–E; Dark blue crosses). While Turbidity and Chl-a data were reviewed for each lake, they were not incorporated into the statistical analyses conducted within this study, as the effective removal of plume-impacted observations (90%) suggests that these datasets were less susceptible to the systematic bias

subsequently noted in the LSWT. The reduced availability of "plume-impacted" observations also reduced our capability to distinguish statistically robust conclusions from these data.

A detailed review of Lake Maihue (HYLA-15083) was conducted as representative of the observed effects of plumes on lake observations. Lake Maihue is one of the closest lakes to the volcano, located ~30 km from the volcanic vent and the highest number of MISR-observed plume/lake intersections (Figure 3). Figure 3B denotes instances where MISR-observed plumes impacted Lake Maihue (Dark Blue notations), with LSWT (Chl-a; Turbidity) observations being screened out in 9/12 (11/12; 11/12) MISR plume occurrences. The remaining three events for LSWT, in June & August 2011 and March 2012, remained consistent with "typical" values derived from historical averages (Figure 3B—Grey). There was only one day in which MISR-observed plume impacted days resulted in a measurement of turbidity and Chl-a (Dec 29th 2011). While the Chl-a does not appear impacted, the Turbidity is ~30% higher than the maximum expected value. While the cloud screening appears broadly effective when considering only the MISR-observed plumes, there are periods when data values fall outside the typical range but did not correspond to MISR-observed plume/lake intersections (Figure 3B—blue dashed area). A subsequent MODIS data review across the eruption period identified more persistent plume presence (see Supplementary material). When the MODIS visual analysis is expanded to the 302 days of the eruption the cause of these outliers becomes evident (Figure 3B). Of the seven outliers recorded between November and February, six were identified with MODIS imagery to have a plume directly over the lake on the day of observation. There was also an instance in March 2012 indicating the plumes continued to impact measurements even as plume became more diffuse. In the Turbidity measurements all four of the outlying observations were impacted by the presence of a volcanic plume (note: one turbidity measurement [Sept 25 2011] was impacted by both meteorological cloud and volcanic plume and is represented by a marker that is half blue and half white). It was also observed that there were times when clouds were present, but a measurement was still provided (Jun and Sep 2011). These observations highlight that the current method for screening out clouds is not always effective for either volcanic plumes or some meteorological clouds. Where these data are interpreted without an understanding of the underlying context or interference present, misrepresentation of the state of the environmental system is likely to occur. This would suggest the need to develop and deploy a quality flag to lake observations that are impacted by volcanic plumes.

There are two plausible possibilities for lake LSWT observations to be impacted by volcanic emissions, which could be occurring independently or concurrently. Firstly, plumes may be too diffuse to observe at the spatial scales employed, even when viewing a longer path length (e.g. that provided by MISR DF and DA cameras; examples provided in the supplemental material), but may continue to impact lake observations. Alternatively, particles emitted from the volcano have been deposited into the lake and are having an ongoing impact on the lake quality parameters observed. While direct field observations of particle deposition and lake chemistry would be required to independently assess this latter mechanism, the temporal behavior of the available satellite observations provides an opportunity to assess whether persistent deposition provides a consistent explanation for the observed anomalies. This assessment is necessarily indirect, and the relative contributions of atmospheric plume interference and deposited volcanic material cannot be independently established without field observations. If the identified temperature shift was the result of deposited particles, then we would expect these outlier variables to occur across all observations in the affected time period at impacted lakes not just those corresponding to the presence of atmospheric plumes, pattern was not consistently observed, with the anomalies instead corresponding to observations of a plume or cloud. However, it was noted that observations were at the upper end of the expected range in the summer months at multiple lakes (Figure 4B, D, F, H). This was a pattern observed in LSWT records irrespective of proximity to the volcano. These higher-skewed temperatures in southern hemispheric summer are interpreted as the result of meteorological warming, as opposed to volcanological interference. Investigation of the climatological record of Chile indicated that 2011 represented the beginning of a 12-year period in which the country experienced above average temperatures every year (IEA 2024). The sporadic nature of the anomalies and their temporal correspondence with the presence of volcanic plumes identified in the MODIS data record therefore provide greater support for atmospheric plume interference as an explanation for the outlying observations, although a contribution from deposited volcanic material cannot be excluded.

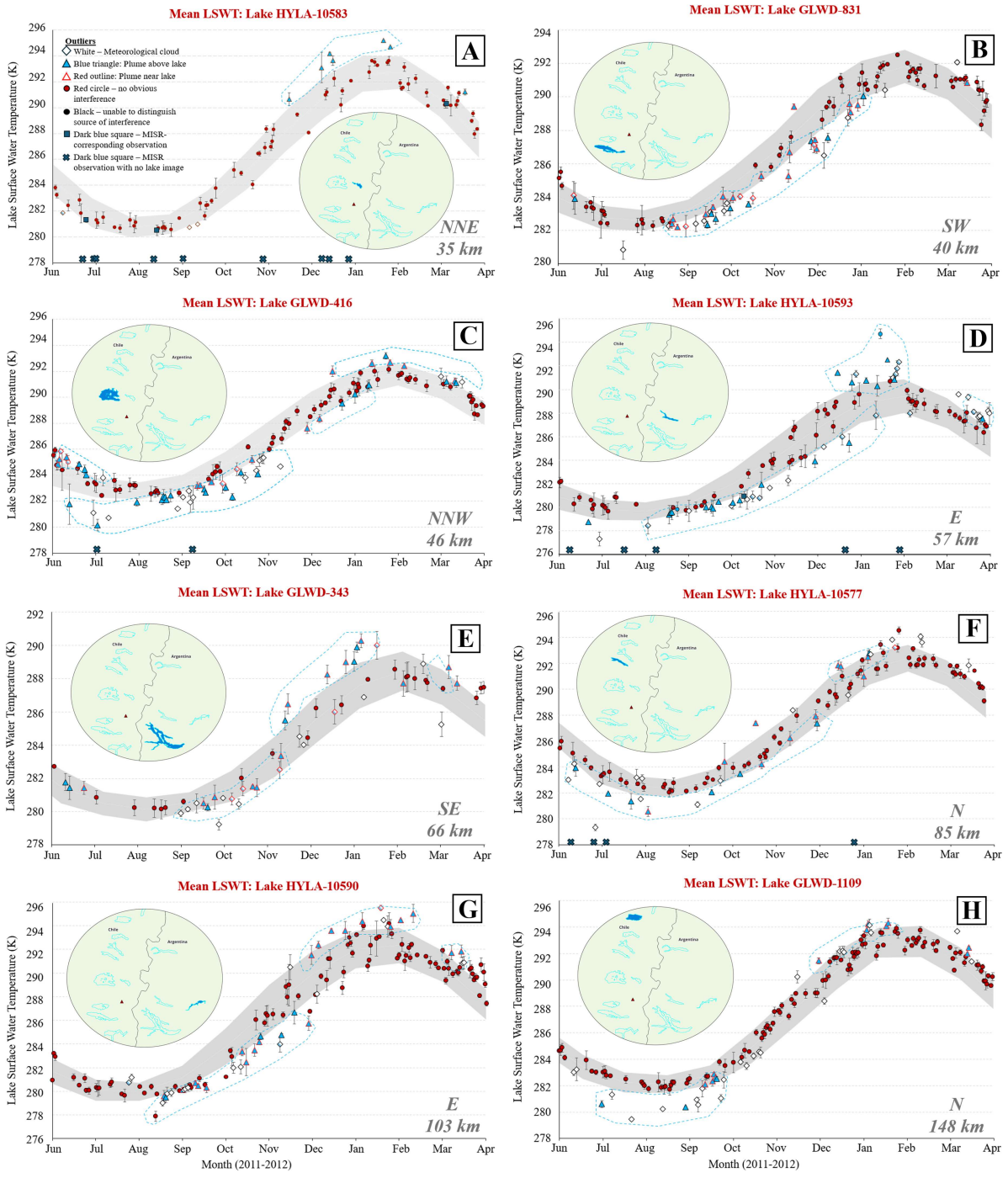


Figure 4. Timelines of remote lake temperature observations for the inter-eruption period of PCC (June 2011–April 2012). Graphed observations (markers) are overlaid on expected monthly values (grey), derived from the average and standard deviation calculated across non-eruption years (2000–2020, inclusive). Outlying values were categorized by potential interference factors (blue triangle—volcanic plume; white diamond—cloud; with red outlines—feature near but not directly over in visual imaging for observation date). Individual lake location maps are included per plot with the corresponding lake highlighted in light blue, with the distance and direction to the lake center point is noted on each plot. Note: Temperature scales vary per plot.

To assess the wider-scale impacts of the plume, the visual analysis was extended to a further seven lakes in close proximity to the volcano. A similar, and in some cases, more pronounced pattern, was observed across the region (Figure 4A–H). In multiple cases, all outliers highlighted between September 2011 and February 2012 occurred on days when a plume was present over, or in close proximity to, the lake (Figure

4B–E). The observation of effects even when the plume is not directly over the lake suggests that diffuse plumes are having an impact on remote lake measurements even when direct observation of the plume over the lake is not discernible (Figure 4A–H: blue triangle with red outline). The statistical analyses performed in Section 4.2 will explore these apparent correlations further.

4. Discussion

The initial results of this analysis highlighted visual evidence that the presence of transient volcanic plumes are having an impact on corresponding remote lake measurements. The remainder of this paper will investigate the significance of the patterns observed and posit the impacts and future directions for this research.

4.1. Proximity analysis

The distance of a particular lake from the center of volcanic activity appears to correlate to the number of observations that are filtered from the Lake CCI database (Figure 4). The PCC eruption occurred over 302 days. Sample locations were included from a range of distances (30–1000 km from the source) to assess the impact of sporadic plume transport on locations with varying impacts.

On average, non-plume impacted periods (standardized to the eruption start and end dates) in this region have ~240 observations per lake with most cases screen out due to cloud. Our proximity analysis (Figure 5A) highlighted that for lakes closest to the volcano this count dropped to ~85 (35 km from source) with a broadly linear increase in observations with distance from the volcano to ~160 (150 km from source) (Figure 5Ai). Those lakes located further than 300 km from the source showed minimal/no effect of the transient plumes. Based on the data available from this location we provisionally propose that a threshold of 270 km be applied (based on the intersection of trendlines from impacted/non-impacted clusters: Figure 5Aii), beyond which we would not expect to see an impact from the volcano. Due to the limited number of lakes located in the 160–290 km distance range (Figure 5Aiii) in this region, we are unable to determine this distance threshold for plume influence with greater accuracy. The lakes were further segregated by direction from source (N, NE, E, SE, S and SW) to identify any effects that could be attributed to local meteorological variations (Figure 5Bii), such as known variations in the persistence and type of cloud features on either side of the Andes (Viale et al. 2019). The results indicate that irrespective of dispersion direction lake observations reductions broadly aligned with the distance from the source, but variability exists that is not explained by distance or direction alone (5Bi-iii). Therefore alternative explanations for observed variations were considered.

In theory, smaller lakes are more susceptible to being completely obscured by a plume if it is present, while larger lakes may remain at least partially visible therefore size should also be considered. Our results highlight that availability of LSWT records increased as lake surface area increased (Figure 5Bi). The spread of this data suggested that size alone did not control overall data availability. Consequently, we investigated the location of the lake relative to the volcano, in addition to lake area of the lakes. Dispersion direction and lake shape appeared to explain the spread of the data, with four groupings identified: Distant Lakes (Far), Northern/Narrow Lakes (North), Western/Broad Lakes (West); and the Outlier Lake (Figure 5Bii). While all three multi-lake groups show greater impact on smaller narrower lakes, the impact was observed to decrease with distance from the source, with trends showing log-linear characteristics with R^2 values of 0.96–0.99 (Figure 5Bii). The rate at which increasing lake size moderates the impact of plumes varies by group. Broad lakes to the west and the outlier lake to the east, show the most significant reduction in observations due to plumes. This greater susceptibility may relate to topographic constraints. Non-buoyant plumes and remobilized ash can become topographically constrained, channeling particles down valleys and into river channels (Flower et al. 2017b; Poulidis et al. 2018; Rave-Bonilla et al. 2023). At PCC, this may have channeled particulates to the "Broad Lakes" to the west, or down towards Nahuel Huapi (outlier: GLWD_343) to the east. However, plume-dispersion and wind modeling were not undertaken in this study, and the role of topography in producing these patterns remains an interpretation rather than a demonstrated mechanism. The variation in the influence observed in these results prevents the development of a simple, but accurate, plume-impacted-lake flag in this region. While it was beyond the scope of this study,

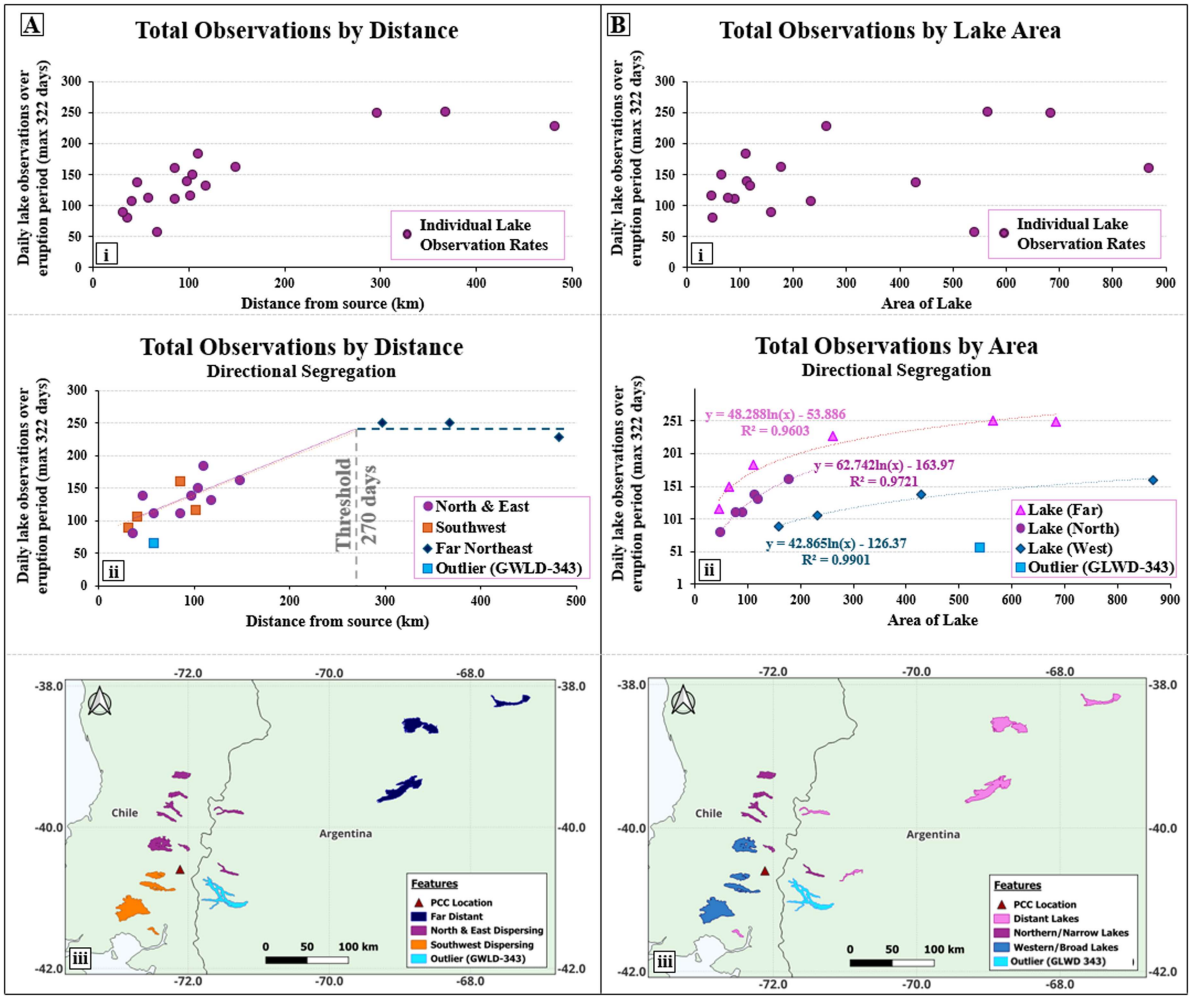


Figure 5. (A) The number of LWST lake observations provided by the Lake CCI database when compared to: (i) distance and (ii) direction from the source, with the average expected observations rate (2000–2010, 2013–2020) indicated by the dashed blue line and the threshold indicated by the gray line; and (iii) corresponding lake location map for groupings; & (B) (i) lake size and (ii) shape/distance groupings, specifically Distant Lakes (Far), Northern/Narrow Lakes (North), Western/Broad Lakes (West); Outlier Lake (GLWD_343), with associated log-linear trendlines, equations, and R^2 values and iii) corresponding lake map highlighting the groupings graphed.

future work should include plume dispersion modeling to investigate how topography influenced plume dispersion during this eruption. Although, a crude data flag identifying observations within 270 km of the volcanic source could be employed, it would result in a significant number of false flags across the region due to topographic influences. Further, the threshold derived here may not be appropriate in other locations.

4.2. Efficacy of existing masking procedures

To assess the significance of the impacts of plumes on LSWT data, identified in Section 3.2, a LMM was employed (see Supplementary data for code and statistical output). These analyses identified that plumes/clouds had more extreme standardized anomalies (Figure 6A) and overall had statistically significant influence on LSWT anomaly values (ANOVA: $F_{1,1347} = 15.66$, $p < 0.001$). The impacted LSWT observations had significantly lower standardized anomalies than non-impacted observations ($\beta = -0.220 \pm 0.056$ SE, $t = -3.96$, $p < 0.001$). However, upon visual inspection of the data (Figure 4A–H) it can be seen that the cloud observations had a greater negative impact than plume-impacted days. The analysis also noted a seasonal effect within the data which required further exploration. While the results were statistically

significant, they highlight only a moderate impact (−0.22 standard units) on the LSWT data, with significant variation between individual observations.

To assess the plume only effect, a subsequent analysis removed the cloud-impacted observations before re-running the analysis. These results showed non-significant effects of plumes on LSWT when no seasonality was considered (ANOVA: $F_{1,1155} = 1.65$, $P = 0.200$). Plume days indicated slightly lower values, but these were not statistically significant. However, visual inspection (Figure 4A–H) and statistical tests highlighted seasonal variability across the LSWT times series. Therefore, an additional analysis was conducted to classify time varying effects.

A LMM with the LSWT as the response variable, and plume impact, month and their interactions included as fixed effects was developed. Lakes were included as a random intercept, allowing a separate estimation of individual lake anomaly baselines between location, particularly important in this study due to the range of lakes included with widely varying physical characteristics (e.g. depth, surface area, and local climatology). This study identified highly significant interactions between plume impact and month of observation (ANOVA: $F_{9,1193.3} = 14.81$, $P < 0.001$) with impacts varying substantially across the year (Figure 6B). Estimated marginal means were used to reveal seasonal differences in plume effects (Table 1) with a highly significant Impact*Month interaction ($F_{9,1193} = 14.81$, $P < 0.001$) corroborating the visual observation that the influence of plumes changes substantially across the year (Figure 4A–H).

Across the analyzed lakes, the direction and magnitude of plume effects varied. However, the model output highlights that the seasonal patterns, summarized above, were present at all 11 lakes analyzed, with cooler-than-expected LSWT in Southern Hemispheric Winter (July–October) and warmer-than-expected temperatures in Southern Hemispheric Summer (December–March). It is noted that while February fell within the "warmer than expected period" the results were negligible in the LMM results. This is likely a result of a limited number of plumes observed during this period (Figure 2Ai), resulting in a smaller sample size, from which it was not possible to discern an effect. Ultimately, these analyses highlight that the impacts of transient plumes on the remote measurement of LSWT are not insignificant. Therefore, a data flag in these cases would be advisable.

4.3. Plume flag development

A preliminary assessment was conducted to identify if, using the atmospheric particle properties derived from MISR observations, it would be possible to distinguish between plumes and non-plume (clear skies and cloud cover) regions based on the data compiled for this location. The Random Forest (RF) classifier achieved an overall cross-validated accuracy of 78.1% (95% CI: 77.8%–78.3%), which was significantly higher than the no-information rate (51.7%; $P < 2.2 \times 10^{-16}$). The model demonstrated moderate agreement between predicted and observed classes (Cohen's $\kappa = 0.600$). Classification performance varied among the three classes. The model identified Plume observations most effectively, with a sensitivity of 84.6%, specificity of 76.8%, and an AUC of 0.893. Increasing the training sample from 50,000 to larger subsets (up to 350,000) produced only marginal improvements in classification accuracy (2%), indicating that model performance had largely converged. In contrast, the corresponding surrogate decision trees became substantially more complex (see Supplemental material), with additional splits and more branching structures impacting overall interpretability without providing commensurate gains in predictive performance. Consequently, the smaller training subset was considered sufficient to capture the dominant relationships within the data while maintaining a more interpretable decision tree. While the identification of Plumes was the primary aim of this flag the accuracy of the Cloud and Background conditions are also important. Background observations were also classified with good performance (sensitivity = 77.6%, specificity = 84.4%, balanced accuracy = 81.0%, AUC = 0.897). In contrast, Cloud observations showed substantially lower sensitivity (37.3%), although specificity remained high (98.4%), indicating that cloud pixels were infrequently misclassified when absent but were often confused with the other classes when present. The one-versus-rest ROC analysis indicated good discriminative ability for all classes (AUC = 0.838–0.892).

Variable importance analysis identified AOD as the most influential predictor by a considerable margin, followed by REPS, REPA, and FNSP (relevance ratio 9:5:4:4, respectively). AOD generated the first and most influential split in the data. Observations below the AOD threshold of 0.154 were predominantly classified as background (75%) and observations above this value were predominantly plumes (69%). Providing a

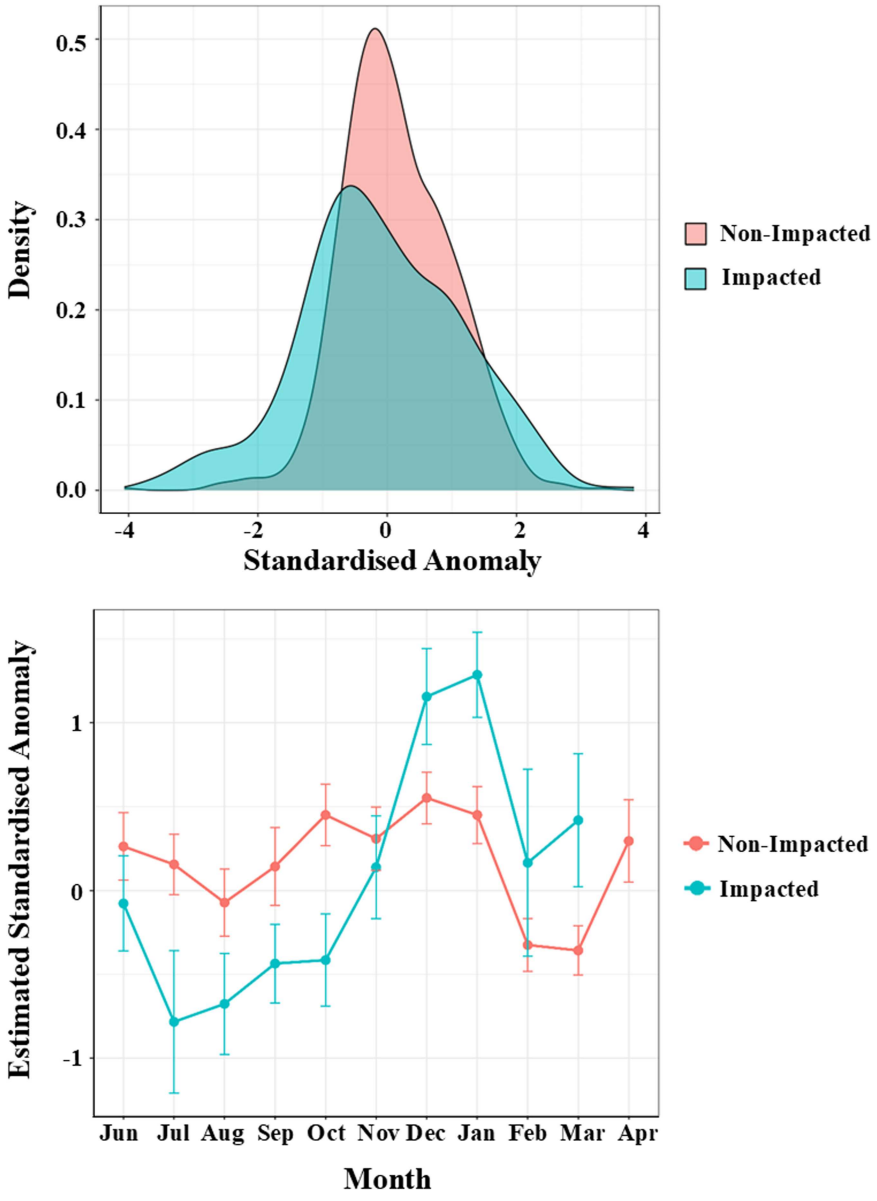


Figure 6. (A) Z-score density plot of standardized anomalies for impacted and non-impacted lake observations; (B) Comparison of monthly estimated standard anomaly for lake surface water temperature between plume impacted and non-impacted observations.

Table 1. Monthly differences in estimated standardized lake surface temperature anomalies between non-impacted and plume-impacted observations, derived from the linear mixed-effects model. Differences represent estimated marginal mean contrasts (non-impacted – impacted), with associated *p*-values. The apparent effect indicates whether plume presence was associated with relatively warmer or cooler lake surface temperatures.

Month	Difference (non−impacted)	*p*-value	Interpretation	Apparent plume effect
January	−0.836	4.6×10^{-8}	Largest positive plume effect	Warming
October	0.865	1.9×10^{-7}	Strong negative plume effect	Cooling
July	0.939	5.9×10^{-5}	Strong negative plume effect	Cooling
December	−0.604	2.0×10^{-4}	Strong positive plume effect	Warming
March	−0.777	2.7×10^{-4}	Strong positive plume effect	Warming
September	0.578	4.7×10^{-4}	Negative plume effect	Cooling
August	0.604	8.8×10^{-4}	Negative plume effect	Cooling
June	0.34	0.051	Borderline	Negligible
February	−0.490	0.095	Not significant	Negligible
November	0.17	0.35	No evidence of an effect	Negligible

simple but generally effect threshold for the flagging of plume/non-plume events. Plumes within an intermittent AOD threshold range of 0.154–0.353 can be combined with FNSP values < 0.0051 to further distinguish background values. For observations with an AOD ≥ 0.353 a threshold of FNSP ≥ 0.0051 can be used to separate pure plume values for those with a cloud component. REPA ≥ 0.910 within the low-FNSP branch favored background, with REPA < 0.910 increasing the probability of an observation being a plume feature. Similarly, REPA < 0.973 combined with REPS ≥ 0.121 identified a terminal node that was 87.6% Plume, while REPS < 0.121 identified a node that was 97.2% Background. Cloud observations were primarily associated with high REPS values (≥1.25 and particularly ≥ 1.99) combined with high AOD (≥0.353) and low FNSP (<0.0051).

The plume flagging process can be summarized by the following steps (Figure 7D):

- AOD ≥ 0.154, especially AOD ≥ 0.353
- FNSP ≥ 0.0051
- REPA is below 0.910–0.973
- REPS is above 0.121 µm

The emphasis on larger particle size (higher REPS), grater angularity (higher FNSP) and more absorbing components (lower REPA) identified with MISR, is indicative of ash components in volcanic plumes (Flower and Kahn 2020). This may cause the developed flag to only be applicable to ash-rich plumes. The composition variability of volcanic plumes would decrease the effective application of the derived flag, specifically as plumes shift from ash-dominated to sulfate-dominated components leading to a decoupling between the expected composition (large, absorbing particles) and that of the sulfate plume (small, spherical, non-absorbing characteristics: Flower and Kahn 2020). The configuration of this flag suggests it would be most effective in locations where plumes contain a significant ash component and would be less effecting where sulfate/water emission dominate like Kilauea, Hawaii and Holuhraun, Iceland (Flower and Kahn 2020, 2021). While there may be issues associated with volcanic sulphate emissions being missed by this flag, similarities in MISR RA retrievals of wildfire smoke, having high AOD and comprised of components up to 0.46 µm (Junghenn Noyes et al. 2020) and dust storms, characterized by AOD in excess

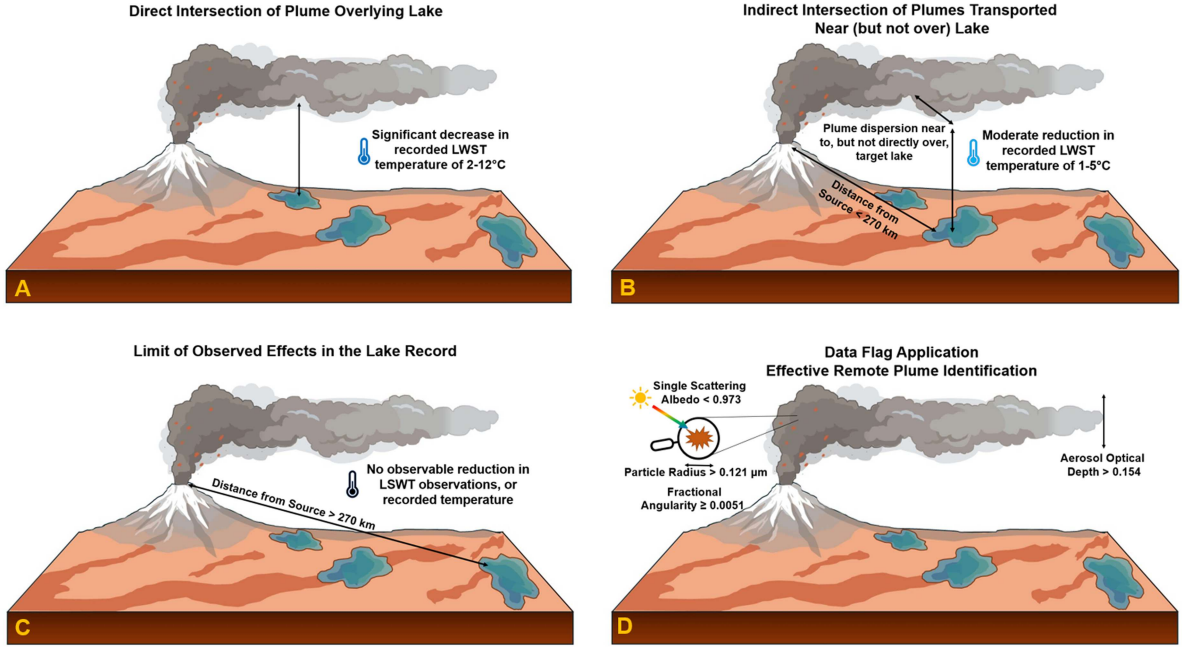


Figure 7. Illustrative model of observed impacts of volcanic plumes on lake surface water temperature (LSWT) for: (A) direct intersection of lakes and plume observations; (B) near-but-not-over-lake plume observations; (C) lakes over 270 km from volcanic source show no impacts due to volcanic plumes; and (D) illustration of plume characteristics vital for automated data flagging.

of 1 and large (>1 µm) angular components (Kahn and Limbacher 2025), suggest that the developed flag may also be applicable alternative transient atmospheric features. More research, incorporating a wider range of volcanic eruptions, is required to establish whether an effective flagging procedure could be employed for lake observations flagging in diverse volcanic regions, as well as to establish if it would also be effective at flagging wildfire smoke or dust storms events.

4.4. Pixel scale impacts

An in-depth analysis of plume impacts on lake observations was conducted at Lake Ranco (GLWD_416) (Figure 8). The results indicate that the influence varied depending on the density and composition of the plume present above the lake. During the early period of the eruption, when dense ash was more prevalent in the plume, lake observations were obscured, resulting in no data. However, in several cases lake observations were still available for areas impacted by a plume. In these cases, LSWT values displayed anomalies of up to −12 °C (Figure 8A and B). This is likely to reflect the influence of the plume on the thermal channels used to calculate LSWT (Carrea et al. 2023). Volcanic plumes are known to contribute interference in the thermal channels due to the specific absorption and scattering properties of common volcanic plume components (e.g. ash and sulfates) (Sellitto et al. 2023).

Later in the eruption period (12th January 2012), when plume observations shifted to water/sulfate-dominated emissions (see Supplementary information), the plume region was effectively masked out (Figure 8C). However, some lower-than-expected values were identified at the plume edge, suggesting that part of the plume was too diffuse to be resolved by remote sensing techniques but sufficiently dense to attenuate the lake signal. The final plume of the eruption period was identified in March (Figure 8D). MODIS observations indicate a narrow core of particles with MISR providing greater context, by revealing a fringe of diffuse particles around the central plume core (see supplementary material for examples of MODIS and MISR imagery). Pixel-level data were retrieved for the majority of the lake area. These observations highlight variations in the response associated with differences in plume density. Where the core of the plume overlaid the lake, the surface temperature observation was characterized by a reduction of ~2 °C, while the region impacted by the more diffuse plume indicates a reduction in recorded surface temperature by ~1 °C (Figure 8D).

When the observations at the lake scale and the pixel scale are combined we can infer three broad categories and their corresponding impacts (Figure 7A–C): lakes directly obscured by ash-rich plumes exhibited large reductions in lake temperature (4 °C–12 °C) where LSWT observations are available (Figure 8A–B); lakes near but not directly below plumes exhibited a moderate reduction in temperature (1 °C–5 °C) (Figure 8C–D); and lakes farther than 270 km from the source showed no evidence of impacts (Figure 5A).

5. Conclusion

This paper has overviewed the investigation of the impact of volcanic plumes, generated from a single volcanic source, on the remote observation of lake water quality parameters from space-borne instruments. The analyses indicate that while dense plumes are often screened out of the observation record (for LSWT, Turbidity and Chlorophyll-a), plumes that are too diffuse to trigger the integrated cloud mask they represent a significant source of uncertainty in satellite-derived lake surface water temperature observations. Using the prolonged 2011–2012 PCC eruption as a case study, we combined ESA CCI Lake products with MODIS and MISR observations to quantify how volcanic aerosols impacted lake surface temperatures across 17 lake systems. The analyses show that current operational cloud masking procedures successfully remove most dense ash-rich plumes, however where masking was not effective LSWT displayed anomalies of up to a 12 °C. The cloud masking procedure frequently failed to identify more diffuse volcanic plumes in the region. These diffuse plumes were associated with biases in satellite-derived lake water quality observations, particularly LSWT, with observed anomalies of 1 °C–5 °C. Linear mixed-effects modeling revealed that the effects of plumes on LSWT were seasonally dependent, generating a cooling effect in winter months and warming effects in the summer. The variability in impact based on both plume characteristics and time of observation prevents the development of a single uniform correction factor for these observations.

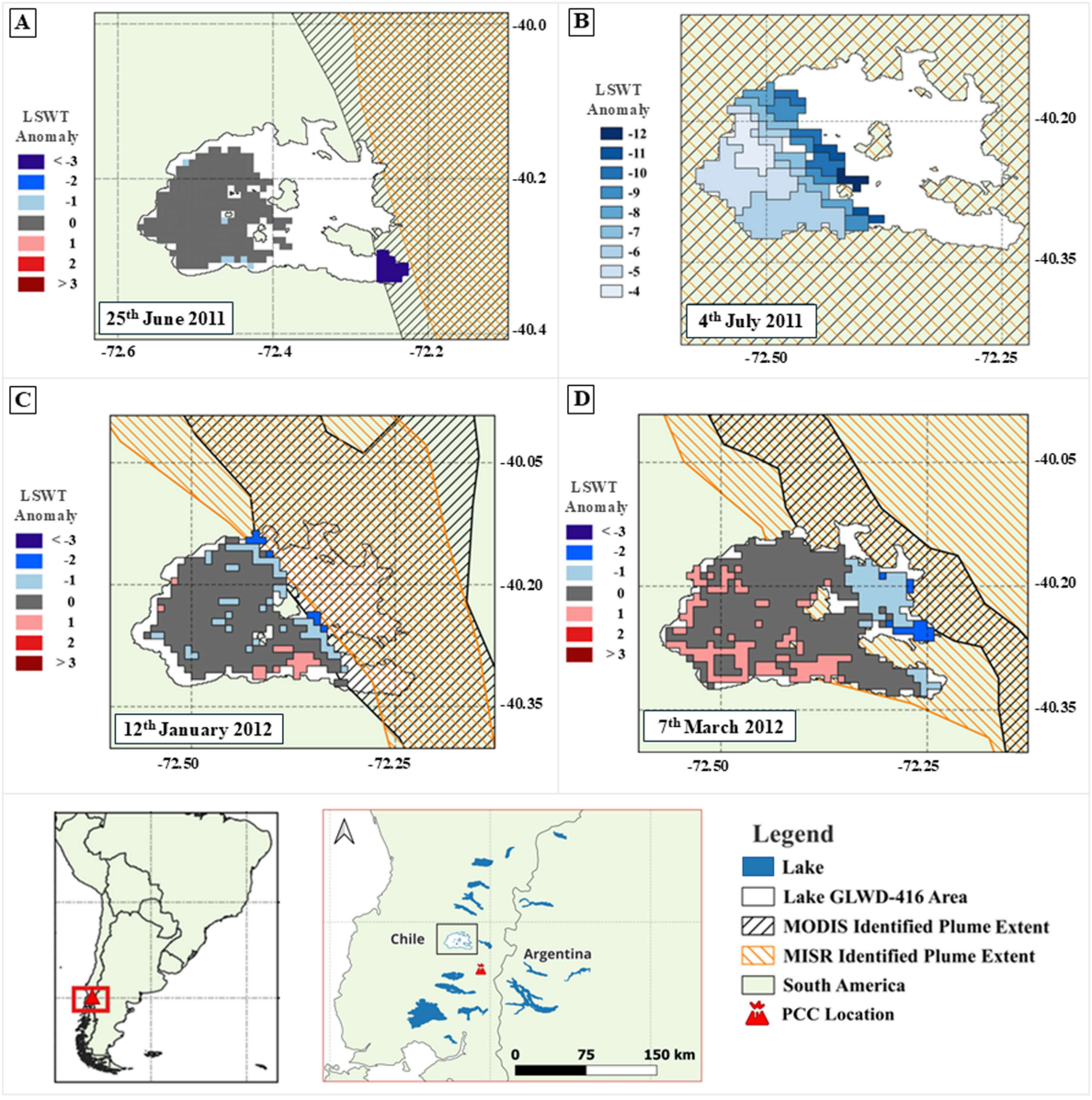


Figure 8. Pixel-level data of lake temperature anomaly (degrees from 2000–2020, non-plume-impacted average) for Lake GLWD_416 (Ranco Lake, Chile), with indications of the location and extent of plumes imaged by the MODIS (gray) and MISR (orange) on four key dates (A) 25th June; (B) 4th July; (C) 12th January; and (D) 7th March. These pixel scale observations provide context for the lake scale observations made earlier in this analysis (Figure 4a–h). The varying impacts of plumes overlaying lakes when observed by optical satellite instruments results in a wider range of observation values, relative to the density of the overlying plume. At the lake scale, this manifests as a wider standard deviation in the observations (Figure 4A–H—vertical error bars) when compared to unaffected lake observations.

The spatial analyses further highlighted the varying influence of volcanic plumes, with not only distance from the volcanic source but also prevailing meteorology, plume characteristics, and lake morphology influencing the impact observed on lake observation records. Topographic channeling may also have contributed to the observed spatial patterns, although this mechanism was not directly tested. Although plume influence appears to become negligible beyond ~270 km in the case of the 2011–2012 PCC eruption, regional variability prevents the adoption of a simple distance-based flag for potentially impacted data. The random forest classification developed here successfully distinguished volcanic plume, cloud and background conditions with an overall accuracy of 78%, highlighting the potential for the future development of a quality flag. Further validation across other eruptions, geographical regions, seasons, lake types and satellite sensors is required to establish the wider applicability of these findings and support the

development of a robust quality flag. Further work should also investigate more varied volcanic plume compositions and extend this analysis to other transient atmospheric features, including wildfire smoke and dust storms.

Collectively, the results indicate that diffuse volcanic plumes can introduce biases into satellite-derived datasets under the conditions observed during this eruption, which may be misinterpreted as genuine environmental change if left unidentified when disseminated. However, the interpretation of these anomalies as atmospheric plume interference is based on their temporal and spatial correspondence with observed volcanic plumes, rather than independent field validation. In the absence of direct measurements of ash deposition and lake chemistry, a contribution from deposited volcanic material cannot be definitively excluded. Due to the complexity of this issue, it requires further study before a flag can be generated for inclusion in the CCI Lake database. However, similarities between MISR-derived particle properties of volcanic plumes, wildfire smoke and dust storms suggest that there is scope to expand this analysis to incorporate a range of transient plume sources.

Acknowledgments

This research was supported by the European Space Agency Lakes Climate Change Initiative grant [CLS-SPA-BC-18-00069] project to VF, DJ & ES. We acknowledge NASA for providing the MISR and MODIS data, with MISR RA plume processing for PCC originally supported by a NASA ROSES 2018 grant [NNH18ZDA001N-ESI] to VF.

Author contributions

CRediT: **Verity Flower:** Conceptualization, Data curation, Formal analysis, Funding acquisition, Investigation, Methodology, Project administration, Validation, Visualization, Writing – original draft, Writing – review & editing; **Dalin Jiang:** Data curation, Project administration, Writing – review & editing; **Evangelos Spyrakos:** Conceptualization, Funding acquisition, Writing – review & editing.

Disclosure statement

No potential conflict of interest was reported by the author(s).

Funding

This research was supported by the European Space Agency Lakes Climate Change Initiative grant [CLS-SPA-BC-18-00069] project to VF, DJ & ES. We acknowledge NASA for providing the MISR and MODIS data, with MISR RA plume processing for PCC originally supported by a NASA ROSES 2018 grant [NNH18ZDA001N-ESI] to VF.

ORCID

Dalin Jiang http://orcid.org/0000-0001-5676-5860
Evangelos Spyrakos http://orcid.org/0000-0001-7970-5211

Data availability statement

While the core data was obtained from public repositories for the completion of the paper. The derived plume outputs, including MISR RA output files, can be found in the following repository: Cordon Caulle Plume Data (2011–2012) – MISR/MODIS Satellite Retrievals https://doi.org/10.5281/zenodo.18990513. The data should be cited as follows: Flower (2026). Cordon Caulle Plume Data (2011–2012) – MISR/MODIS Satellite Retrievals [Data set]. Zenodo. https://doi.org/10.5281/zenodo.18990513.

AI usage statements

Generative AI was used in this study to aid in coding tasks. Specifically, ChatGPT was used to debug coding sections, when errors occurred running the code, and it was also employed to add annotations to coding scripts to ensure that those included in the supplementary material could be understood and used to replicate this study. All suggestions were carefully reviewed by the authors, and no sections of text were directly incorporated into the manuscript based on AI Generated content.

References

Auchmann, R., F. Arfeuille, M. Wegmann, J. Franke, M. Barriendos, M. Prohom, S. Brönnimann, et al. 2013. "Impact of Volcanic Stratospheric Aerosols on Diurnal Temperature Range in Europe over the Past 200 Years: Observations Versus Model Simulations." *Journal of Geophysical Research: Atmospheres* 118 (16): 9064–9077. https://doi.org/10.1002/jgrd.50759.

Ballari, D., L. M. Vilches-Blázquez, M. L. Orellana-Samaniego, F. Salgado-Castillo, A. E. Ochoa-Sánchez, V. Graw, J. Bendix, and N. Turini. 2023. "Satellite Earth Observation for Essential Climate Variables Supporting Sustainable Development Goals: a Review on Applications." *Remote Sensing* 15 (11): 2716. https://doi.org/10.3390/rs15112716.

Bignami, C., S. Corradini, L. Merucci, M. de Michele, D. Raucoules, G. De Astis, J. Piedra, and S. Stramondo. 2014. "Multisensor Satellite Monitoring of the 2011 Puyehue-Cordon Caulle Eruption." *IEEE Journal of Selected Topics in Applied Earth Observations and Remote Sensing* 7 (7): 2786–2796. https://doi.org/10.1109/JSTARS.2014.2320638.

Bolker, B. M., M. E. Brooks, C. J. Clark, S. W. Geange, J. R. Poulsen, M. H. H. Stevens, and J.- S.- S. White. 2009. "Generalized Linear Mixed Models: a Practical Guide for Ecology and Evolution." *Trends in Ecology & Evolution* 24: 127–135. https://doi.org/10.1016/j.tree.2008.10.008.

Bonadonna, C., M. Pistolesi, R. Cioni, W. Degruyter, M. Elissondo, and V. Baumann. 2015. "Dynamics of Wind-Affected Volcanic Plumes: the Example of the 2011 Cordón Caulle Eruption, Chile." *Journal of Geophysical Research: Solid Earth* 120 (4): 2242–2261. https://doi.org/10.1002/2014JB011478.

Breiman, L. 2001. "Random Forests." *Machine learning* 45 (1): 5–32. https://doi.org/10.1023/A:1010933404324.

Carey, S., and M. Bursik. 2015. "Volcanic Plumes, *The encyclopedia of volcanoes*. 571–585. Academic Press. https://doi.org/10.1016/B978-0-12-385938-9.00032-8.

Carrea, L., J. F. Crétaux, X. Liu, Y. Wu, B. Calmettes, C. R. Duguay, C. J. Merchant, et al. 2023. "Satellite-Derived Multivariate World-Wide Lake Physical Variable Timeseries for Climate Studies." *Scientific Data* 10 (1): 30. https://doi.org/10.1038/s41597-022-01889-z.

Carrea, L., Crétaux, J.-F., Liu, X., Wu, Y, Bergé-Nguyen, M, Calmettes, B., Duguay, C, and Jiang, D. 2024. ESA Lakes Climate Change Initiative (Lakes_cci): Lake products, Version 2.1. NERC EDS Centre for Environmental Data Analysis, 04 April 2024. https://doi.org/10.5285/7fc9df8070d34cacab8092e45ef276f1.

Corradino, C., P. Jouve, A. La Spina, and C. Del Negro. 2024. "Monitoring Earth's Atmosphere with Sentinel-5 TROPOMI and Artificial Intelligence: Quantifying Volcanic SO2 Emissions." *Remote Sensing of Environment* 315: 114463. https://doi.org/10.1016/j.rse.2024.114463.

Cutler, A., D. R. Cutler, and J. R. Stevens. 2012. "Random Forests, *Ensemble machine learning*. 157–175. New York, NY: Springer.

Cutler, D. R., T. C. Edwards, Jr, K. H. Beard, A. Cutler, K. T. Hess, J. Gibson, and J. J. Lawler. 2007. "Random Forests for Classification in Ecology." *Ecology (Tempe, AZ)* 88 (11): 2783–2792. https://doi.org/10.1890/07-0539.1.

De'ath, G., and K. E. Fabricius. 2000. "Classification and Regression Trees: a Powerful yet Simple Technique for Ecological Data Analysis." *Ecology (Tempe, AZ)* 81 (11): 3178–3192. https://doi.org/10.1890/0012-9658(2000)081[3178:CARTAP]2.0.CO;2.

Diner, D.J., J.C. Beckert, T.H. Reilly, C.J. Bruegge, J.E. Conel, R.A. Kahn, J.V. Martonchik, T.P. Ackerman, R. Davies, S.A. Gerstl, and H.R. Gordon. 1998. "Multi-angle Imaging SpectroRadiometer (MISR) instrument description and experiment overview." *IEEE Transactions on Geoscience and Remote Sensing* 36 (4): 1072–1087.

Elissondo, M., V. Baumann, C. Bonadonna, M. Pistolesi, R. Cioni, A. Bertagnini, R. Gonzalez, S. Biass, and J. Herrero. 2016. "Chronology and Impact of the 2011 Cordón Caulle Eruption, Chile." *Natural Hazards and Earth System Sciences* 16 (3): 675–704. https://doi.org/10.5194/nhess-16-675-2016. https://nhess.copernicus.org/articles/16/675/2016/.

Fensholt, R., S. Horion, T. Tagesson, A. Ehammer, K. Grogan, F. Tian, K. Rasmussen, et al. 2015. Assessment of Vegetation Trends in Drylands from Time Series of Earth Observation Data. In *Remote sensing time series: Revealing land surface dynamics* 22 159–182, Cham: Springer International Publishing. https://doi.org/10.1007/978-3-319-15967-6_8.

Flower, V. 2026. Cordon Caulle Plume Data (2011-2012) - MISR/MODIS Satellite Retrievals [Data set]. Zenodo. https://doi.org/10.5281/zenodo.18990513.

Fox, E. W., R. A. Hill, S. G. Leibowitz, A. R. Olsen, D. J. Thornbrugh, and M. H. Weber. 2017. "Assessing the Accuracy and Stability of Variable Selection Methods for Random Forest Modeling in Ecology." *Environmental Monitoring and Assessment* 189(7): 316.

Flower, V.J., and R.A. Kahn. 2017a. "Assessing the altitude and dispersion of volcanic plumes using MISR multi-angle imaging from space: Sixteen years of volcanic activity in the Kamchatka Peninsula, Russia." *Journal of Volcanology and Geothermal Research* 337: 1–15.

Flower, V. J., and R. A. Kahn. 2017b. "Distinguishing Remobilized Ash from Erupted Volcanic Plumes Using Space-Borne Multiangle Imaging." *Geophysical Research Letters* 44(20): 10–772.

Flower, V. J., and R. A. Kahn. 2020. "The Evolution of Icelandic Volcano Emissions, as Observed from Space in the Era of NASA's Earth Observing System (Eos)." *Journal of Geophysical Research: Atmospheres* 125 (19): e2019JD031625.

Flower, V. J., and R. A. Kahn. 2021. "Twenty Years of NASA-EOS Multi-Sensor Satellite Observations at Kīlauea Volcano (2000&Ndash2019)." *Journal of Volcanology and Geothermal Research* 415: 107247. https://doi.org/10.1016/j.jvolgeores.2021.107247.

IEA. 2024. National Climate Resilience Assessment for ChileParis: IEA, Licence: CC BY 4.0. https://www.iea.org/reports/national-climate-resilience-assessment-for-chile.

Jiang, D., I. Jones, X. Liu, S. G. Simis, J. F. Cretaux, C. Albergel, E. Spyrakos, and A. Tyler. 2024. "Impacts of Droughts and Human Activities on Water Quantity and Quality: Remote Sensing Observations of Lake Qadisiyah, Iraq." *International Journal of Applied Earth Observation and Geoinformation* 132: 104021. https://doi.org/10.1016/j.jag.2024.104021.

Junghenn Noyes, K., R. Kahn, A. Sedlacek, L. Kleinman, J. Limbacher, and Z. Li. 2020. "Wildfire Smoke Particle Properties and Evolution, from Space-Based Multi-Angle Imaging." *Remote Sensing* 12 (5): 769. https://doi.org/10.3390/rs12050769.

Kahn, R.A., M.J. Garay, D.L. Nelson, K.K. Yau, M.A. Bull, B.J. Gaitley, J.V. Martonchik, and R.C. Levy. 2007. "Satellite-derived aerosol optical depth over dark water from MISR and MODIS: Comparisons with AERONET and implications for climatological studies." *Journal of Geophysical Research: Atmospheres* 112(D18).

Kahn, R. A., and B. J. Gaitley. 2015. "An Analysis of Global Aerosol Type as Retrieved By Misr." *Journal of Geophysical Research: Atmospheres* 120: 4248–4281. https://doi.org/10.1002/2015JD023322.

Kahn, R. A., and J. A. Limbacher. 2025. "Particle Microphysical-Property Evolution in a North African Dust Plume during Trans-Atlantic Transport." *Journal of Geophysical Research: Atmospheres* 130 (16): e2025JD043779.

Kahn, R. A., B. J. Gaitley, M. J. Garay, D. J. Diner, T. Eck, A. Smirnov, and B. N. Holben. 2010. "Multiangle Imaging SpectroRadiometer Global Aerosol Product Assessment By Comparison with the Aerosol Robotic Network." *Journal of Geophysical Research* 115: D23209. https://doi.org/10.1029/2010JD014601.

Kahn, R. A., E. Andrews, C. A. Brock, M. Chin, G. Feingold, A. Gettelman, P. Stier, et al. 2023. "Reducing Aerosol Forcing Uncertainty By Combining Models with Satellite and Within-The-Atmosphere Observations: a Three-Way Street." *Reviews of Geophysics* 61 (2): e2022RG000796. https://doi.org/10.1029/2022RG000796.

Katsev, I. L., A. S. Prikhach, E. P. Zege, and A. A. Kokhanovsky. 2021. "A Robust Atmospheric Correction Procedure for Determination of Spectral Reflectance of Terrestrial Surfaces from Satellite Spectral Measurements." *Remote Sensing* 13 (9): 1831. https://doi.org/10.3390/rs13091831.

Kimball, J. S. 2008. "Earth Observation of Global Change: the Role of Satellite Remote Sensing in Monitoring the Global Environment." *Eos, Transactions American Geophysical Union* 89 (32): 294–294. https://doi.org/10.1029/2008EO320009.

Laiolo, M., M. Ranaldi, L. Tarchini, M. L. Carapezza, D. Coppola, T. Ricci, and C. Cigolini. 2016. "The Effects of Environmental Parameters on Diffuse Degassing at Stromboli Volcano: Insights from Joint Monitoring of Soil CO2 Flux and Radon Activity." *Journal of Volcanology and Geothermal Research* 315: 65–78. https://doi.org/10.1016/j.jvolgeores.2016.02.004.

Lara, L. E., H. Moreno, J. A. Naranjo, S. Matthews, and C. P. De Arce. 2006. "Magmatic Evolution of the Puyehue–Cordón Caulle Volcanic Complex (40 S), Southern Andean Volcanic Zone: from Shield to Unusual Rhyolitic Fissure Volcanism." *Journal of Volcanology and Geothermal Research* 157 (4): 343–366. https://doi.org/10.1016/j.jvolgeores.2006.04.010.

Lessels, J.S., and T.F.A. Bishop. 2013. "Estimating water quality using linear mixed models with stream discharge and turbidity." *Journal of Hydrology* 498: 13–22.

Li, J., B. E. Carlson, Y. L. Yung, D. Lv, J. Hansen, J. E. Penner, Y. Dong, et al. 2022. "Scattering and Absorbing Aerosols in the Climate System." *Nature Reviews Earth & Environment* 3 (6): 363–379. https://doi.org/10.1038/s43017-022-00296-7. https://www.nature.com/articles/s43017-022-00296-7.

Limbacher, J. A., and R. A. Kahn. 2014. "MISRresearch-aerosol-algorithm: Refinements for Dark Water Retrievals." *Atmospheric Measurement Techniques* 7 (1): 1–12. https://doi.org/10.5194/amt-7-1-2014.

Limbacher, J. A., and R. A. Kahn. 2017. "Updated MISR Dark Water Research Aerosol Retrieval algorithm—Coupled 1.1 Km Ocean Surface chlorophyll-a Retrievals with Empirical Calibration Corrections." *Atmospheric Measurement Techniques* 10 (4): 1539–1555. https://doi.org/10.5194/amt-10-1539-2017.

Maes, K., S. Vandenbussche, L. Klüser, N. Kumps, and M. De Mazière. 2016. "Vertical profiling of volcanic ash from the 2011 puyehue cordón caulle eruption using IASI." *Remote Sensing* 8 (2): 103.

Martonchik, J. V., R. A. Kahn, and D. J. Diner. 2009. Retrieval of Aerosol Properties over Land Using MISR Observations. In *Satellite aerosol remote sensing over land* A Kokhanovsky, ed. 267–291, Berlin: Springer. https://doi.org/10.1007/978-3-540-69397-0_9.

Moroney, C., R. Davies, and J. P. Muller. 2002. "Operational Retrieval of Cloud-Top Heights Using MISR Data." *IEEE Transactions on Geoscience and Remote Sensing* 40 (7): 1532–1540. https://doi.org/10.1109/TGRS.2002.801150.

Muller, J. P., A. Mandanayake, C. Moroney, R. Davies, D. J. Diner, and S. Paradise. 2002. "MISR Stereoscopic Image Matchers: Techniques and Results." *IEEE Transactions on Geoscience and Remote Sensing* 40 (7): 1547–1559. https://doi.org/10.1109/TGRS.2002.801160.

National Academies of Sciences (NAS), Medicine, Division on Earth, Life Studies, Board on Earth Sciences, Committee on Seismology, & Committee on Improving Understanding of Volcanic Eruptions. 2017. *Volcanic eruptions and their repose, unrest, precursors, and timing*. National Academies Press.

Nelson, D. L., M. J. Garay, R. A. Kahn, and B. A. Dunst. 2013. "Stereoscopic Height and Wind Retrievals for Aerosol Plumes with the MISR INteractive eXplorer (Minx)." *Remote Sensing* 5 (9): 4593–4628. https://doi.org/10.3390/rs5094593.

Nelson, D. L., Y. Chen, R. A. Kahn, D. J. Diner, and D. Mazzoni. 2008. "Example Applications of the MISR INteractive eXplorer (MINX) Software Tool to Wildfire Smoke Plume Analyses." *Proceedings of SPIE* 7089(09): 1–11. https://doi.org/10.1117/12.795087.

Newhall, C. G., and S. Self. 1982. "The Volcanic Explosivity Index (VEI) an Estimate of Explosive Magnitude for Historical Volcanism." *Journal of Geophysical Research: Oceans* 87 (C2): 1231–1238. https://doi.org/10.1029/JC087iC02p01231.

Niroumand-Jadidi, M., F. Bovolo, and L. Bruzzone. 2020. "Water Quality Retrieval from PRISMA Hyperspectral Images: First Experience in a Turbid Lake and Comparison with Sentinel-2." *Remote Sensing* 12 (23): 3984. https://doi.org/10.3390/rs12233984.

Pavolonis, M. J., J. Sieglaff, and J. Cintineo. 2018. "Automated Detection of Explosive Volcanic Eruptions Using Satellite-Derived Cloud Vertical Growth Rates." *Earth and Space Science* 5 (12): 903–928. https://doi.org/10.1029/2018EA000410.

Petracca, I., D. De Santis, M. Picchiani, S. Corradini, L. Guerrieri, F. Prata, G. Schiavon, et al. 2022. "Volcanic Cloud Detection Using Sentinel-3 Satellite Data By Means of Neural Networks: the Raikoke 2019 Eruption Test Case." *Atmospheric Measurement Techniques* 15 (24): 7195–7210. https://doi.org/10.5194/amt-15-7195-2022.

Picchiani, M., M. Chini, S. Corradini, L. Merucci, A. Piscini, and F. Del Frate. 2015. "Neural Network Multispectral Satellite Images Classification of Volcanic Ash Plumes in a Cloudy Scenario." *Annals of Geophysics* 57. https://doi.org/10.4401/ag-6638.

Poulidis, A. P., J. C. Phillips, I. A. Renfrew, J. Barclay, A. Hogg, S. F. Jenkins, R. Robertson, and D. M. Pyle. 2018. "Meteorological Controls on Local and Regional Volcanic Ash Dispersal." *Sci Rep-Uk* 8: 6873. https://doi.org/10.1038/s41598-018-24651-1.

QGIS.org. 2025. QGIS Geographic Information System. QGIS Association. http://www.qgis.org.

R Core Team. 2025. *R: A Language and Environment for Statistical Computing*. Vienna, Austria: R Foundation for Statistical Computing. https://www.R-project.org/.

Rave-Bonilla, Y. P., D. E. Jessop, S. Moune, C. Garbin, and R. Moretti. 2023. "Numerical Modelling of the Volcanic Plume Dispersion from the Hydrothermal System of La Soufrière De Guadeloupe." *Volcanica* 6 (2): 459–477. https://doi.org/10.30909/vol.06.02.459477.

Rayborn, L., and A. M. Jellinek. 2022. "Random Forest Predictions of Fine Ash Concentration and Charging Processes from Experimentally Generated Volcanic Discharges." *Journal of Geophysical Research: Solid Earth* 127 (5): e2021JB023599.

Rickards, N., R. Chengot, H. Baron, and M. Fry. 2023. Review of Global in Situ Data for Lakes and Reservoirs. 12. European Environment Agency. https://nora.nerc.ac.uk/id/eprint/537299.

Robbins, D., C. Poulsen, S. Siems, and S. Proud. 2022. "Improving Discrimination between Clouds and Optically Thick Aerosol Plumes in Geostationary Satellite Data." *Atmospheric Measurement Techniques* 15 (9): 3031–3051. https://doi.org/10.5194/amt-15-3031-2022.

Romeo, F., L. Mereu, S. Scollo, M. Papa, S. Corradini, L. Merucci, and F. S. Marzano. 2023. "Volcanic Cloud Detection and Retrieval Using Satellite Multisensor Observations." *Remote Sensing* 15 (4): 888. https://doi.org/10.3390/rs15040888.

Sajib, A. M., M. G. Uddin, A. Rahman, R. Ahmadian, and A. I. Olbert. 2025. "Remote Sensing Applications for Monitoring Optically Inactive Water Quality Indicators: a Comprehensive Review." *Earth-Science Reviews* 271: 105259. https://doi.org/10.1016/j.earscirev.2025.105259.

Salomonson, V. V., W. L. Barnes, P. W. Maymon, H. E. Montgomery, and H. Ostrow. 1989. "MODIS: Advanced Facility Instrument for Studies of the Earth as a System." *IEEE Transactions on Geoscience and Remote Sensing* 27 (2): 145–153. https://doi.org/10.1109/36.20292.

Schielzeth, H., N. J. Dingemanse, S. Nakagawa, D. F. Westneat, H. Allegue, C. Teplitsky, Y. G. Araya-Ajoy, et al. 2020. "Robustness of Linear Mixed-Effects Models to Violations of Distributional Assumptions." *Methods in Ecology and Evolution* 11 (9): 1141–1152. https://doi.org/10.1111/2041-210X.13434.

Scollo, S., R. A. Kahn, D. L. Nelson, M. Coltelli, D. J. Diner, M. J. Garay, and V. J. Realmuto. 2012. "MISR Observations of Etna Volcanic Plumes." *Journal of Geophysical Research* 117: D06210. https://doi.org/10.1029/2011JD016625.

Sellitto, P., G. Salerno, S. Corradini, I. Xueref-Remy, A. Riandet, and C. Bellon, et al. 2023. "Volcanic Emissions, Plume Dispersion, and Downwind Radiative Impacts Following Mount Etna Series of Eruptions of February 21–26, 2021." *Journal of Geophysical Research: Atmospheres* 128 (6): e2021JD035974.

Sheffield, J., E. F. Wood, M. Pan, H. Beck, G. Coccia, A. Serrat-Capdevila, and K. J. W. R. R. Verbist. 2018. "Satellite Remote Sensing for Water Resources Management: Potential for Supporting Sustainable Development in Data-Poor Regions." *Water Resources Research* 54 (12): 9724–9758. https://doi.org/10.1029/2017WR022437.

Silvey, S., and J. Liu. 2024. "Sample Size Requirements for Popular Classification Algorithms in Tabular Clinical Data: Empirical Study." *Journal of Medical Internet Research* 26: e60231. https://doi.org/10.2196/60231.

Simis, S., L. Carrea, B. Calmettes, J.-F. Cretaux, C. Duguay, X. Liu, A. Mangilli, and H. Yesou. 2025. Lakes Climate Change Initiative End-To-End ECV Uncertainty Budget (E3UB) (Version 3.0.0).European Space Agency.

Sparks, R. S. J., M. I. Bursik, S. N. Carey, J. Gilbert, L. S. Glaze, H. Sigurdsson, and A. W. Woods. 1997. *Volcanic plumes*. Wiley.

Tournigand, P. Y., J. J. P. Fernández, J. Taddeucci, D. Perugini, J. Sesterhenn, and D. M. Palladino. 2019. "Time Evolution of Transient Volcanic Plumes: Insights from Fractal Analysis." *Journal of Volcanology and Geothermal Research* 371: 59–71. https://doi.org/10.1016/j.jvolgeores.2018.12.007.

Vera Mercado, J. A., and B. Engel. 2021. "Multi-Scale Analysis of the Dependence of Water Quality on Land Use Using Linear and Mixed Models." *Water* 13 (19): 2618. https://doi.org/10.3390/w13192618.

Vermote, E. F., J. C. Roger, A. Sinyuk, N. Saleous, and O. Dubovik. 2007. "Fusion of MODIS-MISR Aerosol Inversion for Estimation of Aerosol Absorption." *Remote Sensing of Environment* 107 (1-2): 81–89. https://doi.org/10.1016/j.rse.2006.09.025.

Viale, M., E. Bianchi, L. Cara, L. E. Ruiz, R. Villalba, P. Pitte, L. Zalazar, M. Masiokas, and J. Rivera. 2019. "Contrasting Climates at Both Sides of the Andes in Argentina and Chile." *Frontiers in Environmental Science* 7: 69. https://doi.org/10.3389/fenvs.2019.00069.

Wright, R., L. Flynn, H. Garbeil, A. Harris, and E. Pilger. 2002. "Automated Volcanic Eruption Detection Using Modis." *Remote Sensing of Environment* 82 (1): 135–155. https://doi.org/10.1016/S0034-4257(02)00030-5.

Xiao, N., T. Shi, C. A. Calder, D. K. Munroe, C. Berrett, S. Wolfinbarger, and D. Li. 2009. "Spatial Characteristics of the Difference between MISR and MODIS Aerosol Optical Depth Retrievals over Mainland Southeast Asia." *Remote Sensing of Environment* 113 (1): 1–9. https://doi.org/10.1016/j.rse.2008.07.011.

Zeng, L., T. Charoensuk, C. Chewning, D. Druce, C. Toettrup, K. Nielsen, and P. Bauer-Gottwein. 2025. "Exploitation of Satellite Earth Observation Datasets for Hydrologic Analysis of Large Reservoirs in Thailand." *Journal of Hydrology* 659: 133085. https://doi.org/10.1016/j.jhydrol.2025.133085.

Zuur, A. F., E. N. Ieno, N. J. Walker, A. A. Saveliev, and G. M. Smith. 2009. "Limitations of Linear Regression Applied on Ecological Data. In *Mixed effects models and extensions in ecology with R*. 11–33. New York, NY: Springer New York.